Clinical Translation of ^{90}Y-Labeled Hydroxyapatite Particles 7

Production of ^{99}Mo-^{99m}Tc in Accelerator 11

Neutron Studies on Functional Materials 24

Bi-monthly • November - December • 2016

ISSN: 0976-2108

BARC NEWSLETTER

Bioluminescence Image - Page 7

CONTENTS

Founder's Day 2016: Address by
Dr. Sekhar Basu
Chairman, AEC & Secretary, DAE 1

Founder's Day 2016: Address by
K.N. Vyas
Director, BARC
 4

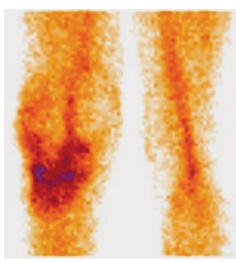

Successful Clinical Translation of ^{90}Y-Labeled Hydroxyapatite Particles Prepared Utilizing ^{90}Y Produced in Dhruva Research Reactor
Sudipta Chakraborty, K.V. Vimalnath, A. Rajeswari, Ashutosh Dash, H.D. Sarma, K. Kamaleshwaran, Ajit Shinto 7

Production of ^{99}Mo-^{99m}Tc Medical Isotopes using Accelerator as an Alternative Route
H. Naik, S.V. Suryanarayana, A. Gopalakrishna, G.N. Kim and Roberto Capote Noy
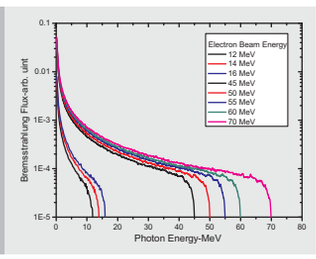

11

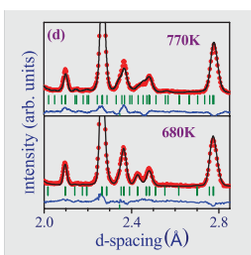

Neutron Scattering Studies of Eco-friendly Functional Materials
S.K. Mishra, M.K. Gupta, R. Mittal, P.S.R. Krishna and S.L. Chaplot 24

Machine Vision Applications for Physical Security, Quality Assurance and Personnel Dosimetry
S. Kar, S.V. Shrikhande and R.M. Suresh babu


29

Sixteenth Training Course on "Crane Operation", organised by Material Handling Equipment Committee of BARC Safety Council 33

Technology Transfer to Industries 34

28th DAE All India Essay Contest 36

Release of the Founder's Day Special Issue of the BARC Newsletter 36

DAE (Excellence in Science, Engineering & Technology) Awards 2015 37

Founder's Day 2016

Address by

Dr. Sekhar Basu

Chairman, AEC & Secretary, DAE

Good morning to all of you, Senior Members of the DAE Family, Distinguished Invitees, Representatives from Media, my dear Colleagues and Friends, I extend warm welcome to all of you, to this Founder's Day celebrations, to pay respectful homage to our visionary Founder, Dr. Homi Jehangir Bhabha, on his 107th birth anniversary. This is a day for us to reflect on our recent performance and achievements and also re-dedicate ourselves to realise the vision of our Founder for the continued development in the field of nuclear energy and nuclear applications, to bring prosperity for all.

Dear Friends,

I will talk about our recent activities; re-grouped as per the document presented to the NITI Aayog on DAE vision, action plan and strategy. Let me start with the first stage of Indian Nuclear Power Programme. In the last budget speech, Honourable Finance Minister has indicated funding to the extent of Rs.3,000 crores on a continuous basis for the nuclear power programme. We have proposed capacity addition of 2.5 to 3 GWe every year for next 15 to 20 years. In addition to about 5.7 GWe power generating capacity, we are also constructing 10 reactors which will add 7.7 GWe by 2024. We have approached the government for sanction of serial construction of 10 PHWRs in one go. The arrangements for Kudankulam Units 5&6 is also likely to be finalised shortly.

You are aware that Kudankulam Unit 1 is performing consistently at full power since February 2016 and Kudankulam Unit 2 has been synchronised to the grid. Construction activity for Kudankulam Units 3&4 has also been started. Recent incident of pressure tube failure in Kakrapar Atomic Power Station Unit 1 proved the excellent performance of our safety systems following the event. Our operators and designers rose to the occasion to handle this incident in Level-1 category without any problems. Both KAPS-1&2 are now taken up for en masse coolant channel replacement (EMCCR). First 700 MWe PHWR, KAPS – 3 is likely to go critical by next year and we expect to commission the other 3 reactors at KAPS and RAPS over the next 3 years. Our Heavy Water Plants worked at 105% capacity and we are exporting heavy water in small quantities to the developed nations. Nuclear Fuel Complex (NFC) created world record last year by producing 1500 Tonnes of PHWR fuel.

Dear Colleagues,

On the Uranium front, I am glad to announce that problems at Tummalapalle has been sorted out and uranium production is increasing in a systematic manner. To increase the overall production in the country, we have started work for opening up new mines at Rohil and Gogi. Uranium exploration in Kadappa basin and North-East is also being stepped up. Recently our exploration activities in Gondwana basin, Betul District of Madhya Pradesh has also given encouraging results. In the second stage of our nuclear power programme,

I am happy to inform that Prototype Fast Breeder Reactor (PFBR) commissioning activity is progressing well. After completion of all system checks and rectifications pressure testing and pre-heating activity prior to sodium filling will be completed by the year end. Regulatory requirements are also being addressed in a systematic manner. I must also mention about the never before performance of our nuclear recycle plants, resulting in delivery of first core for PFBR. Production of fuel for first refuelling of PFBR is in hand. Construction of large sized Integrated Nuclear Recycle Plant, along with fuel fabrication facility has been started at Tarapur. Construction activity for Fast Reactor Fuel Cycle Facility (FRFCF) is also picking up at Kalpakkam.

Dear Colleagues and Friends,

The health care sector, got major boost, with the construction activities for 2 new hospitals at Vizag in Andhra Pradesh and Mohali in Punjab. The facility at Vizag is already providing cancer care in 7 specialised areas from temporary sheds. Through National cancer grid, 85 hospitals have been connected for providing health care support to all the smaller centres and deliver uniform quality of health care throughout the country. A 60 bedded hospital at Sangrur, Punjab, built with the help from State Government, is providing cancer care in 6 specialised areas. We have also started work for creation of Radiation Medicine Research Centre (RMRC) at our Rajarhat campus in Kolkata. After successful launch of cancer App during the last IAEA General Conference, another App for cancer staging for gynaecological cancer care was launched during the IAEA General Conference in Vienna in 2016. BRIT has supplied cesium pencils for blood irradiators for 4 hospitals. Development of cancer drugs for making cancer care affordable is going on well and some of the drugs developed by our scientists are undergoing field trials. On the food security front, We have released TM-108-1 high yielding mustard seed for Maharashtra. Two soya bean mutants resistant to bacteria and virus and one early maturing variety are undergoing trial. 460 quintals of breeder seeds of different TG varieties were distributed in 9 States.

A Gazette notification has been issued for approval of radiation processing of food in May2016. This covers all types

of food products, food packaging material, food additives, for decontamination, disinfection and sterilisation. In the area of water and waste management, increasing popularity of NISARGRUNA has resulted in addition of 15 plants in the last year in various parts of the country. We have taken up projects for treatment of textile dye effluent using a mix of technologies. The feasibility of textile dye effluent treatment using electron beam was demonstrated in small scale at Kharghar. Demonstration facility for effluent treatment by radiation grafting process is being fabricated for trials at Surat and Ahmedabad. Dry sludge hygienisation facility coming up at Ahmedabad will be commissioned next year. We expect more interest in this technology after this plant goes into operation.

Dear Friends,

In Mega Science schemes, Laser Interferometer Gravitational-Wave Observatory (LIGO) has been approved by the government in principle and it has been decided to build the facility at Hingoli, for which Maharashtra government has allocated 40 acres of land and the rest is being acquired. With the shipment of camera, MACE telescope construction got a major boost and now we expect it to be fully commissioned by 2017. Fermilab collaboration for construction of high energy accelerator is making progress and components made in India are being tested at Fermilab for acceptance. Tests conducted so far has given very encouraging results. In the area of basic research and science education, our National Institute of Science Education and Research (NISER) was dedicated to the nation by our Hon'ble Prime Minister in the Month of February 2016.

NISER is offering science education through 5 different schools and is making outstanding contributions to science education, I am glad to announce that Prof. B. Mohanty from this institute was awarded Shanti Swarup Bhatnagar Award 2015 for Physics. HBNI administrative arrangements has been streamlined after the acceptance of HBNI MoA/Rules by Charity Commissioner. National Institute Ranking Framework has ranked HBNI 17th. This is likely to improve substantially once the institute's name is mentioned in the students publication. During this period, Tata Institute of Fundamental Research (TIFR) has discovered superconductivity in pure Bismuth at 500 micro Kelvin. TIFR has also developed 3 out of 5 major instruments being used at ASTROSAT satellite, and they are functioning well. CERN authorities has agreed to the proposal of India joining the CERN programme as Associate Member and the agreement is likely to be signed next month.

Dear all,

In the area of directed research, the following were some of the major developments : Last year Dhruva reactor was operated at highest ever capacity factor and Fast Breeder Test Reactor (FBTR) at Kalpakkam has been operated at highest ever power during this period. Metallic fuel irradiation for future metallic fuel FBRs has been started at FBTR. Synchrotron facility at Indore continue to be used on 24 x 7 basis and all the beamlines are used by scientists and students from all over the country. Country's first infra-red free electron laser is being built in a 60 M shielded tunnel at Indore. Sub-systems for this facility are being tested. Acceleration of protons upto 11 MeV and of carbon ions upto 14.5 MeV has been achieved using ultra-intense Ti:sapphire femtosecond laser.

Director, BARC has already covered the developments in BARC in the area of directed research. Our pavilion at the General Conference in IAEA attracted a large number of students and scientists from all over the world. Many countries expressed desire to collaborate with us in Nuclear application area. Dear Friends, During the 60th year of IAEA at the General Conference, we highlighted the contribution of Dr. Homi Jehangir Bhabha, who was not only the founder of India's atomic energy programme, but also shaped the evolution of IAEA. You may be aware of the fact that Dr. Bhabha had great appreciation for cultural and musical heritage of Vienna. As the Chair of the body entrusted with the responsibility of selection of headquarters of IAEA, Dr. Bhabha used his casting vote for selection of Vienna as IAEA headquarters over Geneva. Some of our other achievements can be summarised as follows:

Atomic Energy Act was amended to make it possible for Nuclear Power Corporation of India Limited (NPCIL) to form Joint Ventures with other PSUs for production of nuclear power. Civil Nuclear Liability issues were addressed by the introduction of Operators' Policy and Suppliers' Policy through India Nuclear Insurance Pool. Ratification of IAEA's Convention on Supplementary Compensation also happened this year. India participated in the Nuclear Security Summit at Washington at the highest political level and is contributing to various global initiatives on combating nuclear terrorism.

Dear Colleagues,

I thank all of you for your achievements. But we have much more to do. It will be worthwhile to tell you about our proposal to NITI Aayog about the 15 year Vision Scheme, 3 year Action Plan and 7 year Strategy. We have proposed 10 schemes with the following vision:

1. Creation of 2.5 to 3 GWe (average capacity) per year for next 15 to 20 years.
2. Ten fold rise in exploration and production of uranium and rare earths to achieve self-sufficiency.
3. Ten fold rise in power from Fast Breeder Reactors (FBR) and creation of matching fuel cycle facilities in the back end.
4. Affordable cancer care for 5 lakh new patients per year and decreasing the cancer mortality rate by 15%.

5. Creation of networks and Facilities to provide food security through nuclear agriculture and food preservation for 10% of the Indian population.
6. Management of Municipal waste in 50 cities and providing water purification facilities for 20000 villages.
7. Completion and uitilisation of various accelerator programmes, India-based Neutrino Observatory (INO), Laser Interferometer Gravitational Observatory (LIGO), European Centre for Nuclear Research (CERN), International Thermonuclear Experimental Reactor (ITER) etc.
8. Pursuing curiosity driven basic research programmes for understanding the fundamental nature of processes, creation of knowledge base and science education.
9. R&D activities directed towards achieving specific objectives of the Department in the nuclear and allied fields.
10. Creation of network for need based social outreach activities in and around DAE facilities and step up awareness programmes for target audience.

Action plan is an integral part of the Vision Document. Presently we are working on elaboration of the action plan. Involvement of other central ministries and state governments will be key to the implementation of these programmes. Improved monitoring will also be essential component of our action plan.

Dear All,

Today, I see growing optimism, both at national and global level, about the growth of Indian nuclear programme. Our COP-21 commitments on carbon emission, and our growth potential in the uranium production, health care and other sectors capable of providing direct benefit to the society; has created great opportunity for us to deliver. Everybody is waiting for us to act.

Thank you and Jaihind

Founder's Day Address

Address by
K.N. Vyas
Director, BARC

Dr. Sekhar Basu, Chairman, AEC, Senior Members of the DAE Family, Distinguished Invitees, Representatives of the Media, my dear Colleagues, Ladies and Gentlemen,

It is indeed a matter of great pleasure and proud privilege for me to extend a warm welcome to all of you to the Founder's Day functions scheduled today.

It has been our tradition to pay respectful homage to our visionary Founder, Dr Homi Jehangir Bhabha, on his birth anniversary, the 30th October every year. The 107th Birth Anniversary of Dr. Bhabha falls over the weekend this year and hence this function is held today. This is an occasion for introspection on our performance and achievements of the past year, as well as to rededicate ourselves to continue to do our best in providing maximum benefits from the application of nuclear science and technology to our great nation and its people.

I will describe about the performance highlights of BARC during the last one year in various areas of our mandate, just to have a glimpse of the typical range and nature of our works and achievements.

I start with some of our achievements in Nuclear Power related R&D, support to NPCIL and Research Reactor.

1. Dhruva Reactor was operated at rated power throughout the year and logged an availability of ~72.7% and a capacity factor of ~64.7%, which is the highest ever since it's commissioning.
2. Retention of core melt within the calandria of PHWR and AHWR has been demonstrated in a fully simulated experimental set up. In addition, a mini core catcher experiment has been completed. Such experiments will provide an independent database for development of our indigenous core-catcher designs. An integrated test of different passive systems was carried out to demonstrate that AHWR can withstand severe accident in case of prolonged station black out up to 7 days.

Our teams made laudable achievements in developing and producing Advanced Nuclear Fuels & Special Materials.

1. For the first time, PIE of two fuel bundles from 540 MWe (TAPS-1&2) reactor have been carried out in New Hot Cell facility, where performance of fuel bundles with 37 fuel elements have been examined.
2. Specific grade of beryllia ceramic having high dielectric constant has been developed for use as heat sink in high power output electronic devices, such as multiplexer for communication satellites.

We continued to make commendable contributions in the field of reprocessing and waste management.

1. PREFRE-2 reprocessing plant at Tarapur continues to give excellent performance and achieved highest ever through-put in the year 2015. Kalpakkam Reprocessing Plant (KARP) performed very well. Advanced vitrification and treatment plants at Tarapur also gave best ever performance in 2015.
2. PHWR spent resin cementation system has been commissioned for the first time in plant scale at WIP Kalpakkam.
3. Multi step solvent extraction process was employed for the separation of high specific activity ^{90}Sr from PUREX-HLLW. This activity was used to separate carrier-free ^{90}Y in acetic acid medium using two stage supported liquid membrane generator system developed in-house, for radiopharmaceutical applications.
4. High resolution Large area silicon detectors for alpha particles have been developed and tested in collaboration at IGCAR for development of Pu in air monitoring at fuel reprocessing/fabrication facilities at IGCAR. Production of these units is underway for large deployment in fast reactor fuel reprocesing plants at IGCAR.

Let me now bring out some of the major outputs of our R&D efforts in Chemical and Physical Sciences

1. A high end two-dimensional infrared spectrometer, first of its kind in India, which offers time resolution of a few tens of femto-second has been developed for advanced studies in chemistry and biology. A laser scanning confocal fluorescence lifetime imaging and single molecule spectroscopy setup has been developed, which is also first of its kind in India.
2. Novel lead-free X-ray shield has been developed by a facile solvent-free procedure which yields cost-effective standalone polymer-ceramic composite sheets. It possesses exceptionally superior mechanical behavior with stretchability of 400% even at a high loading of 80 wt% filler. A sheet of 560 microns could provide an attenuation of 99.5% for X-ray beam at 60 kV.
3. Second stage preclinical trial of DSePA, an indigenously developed radio-protector, has been successfully completed in collaboration with ACTREC.
4. Test facility for production of solar hydrogen using two-step hybrid sulfur thermo-chemical cycle has been developed. The high temperature (800^0C) required for the

thermo-chemical cycle is obtained using a 1.8m dia solar concentrator.

5. In search of super-heavy-nuclei, the average number of prompt neutrons that may be emitted in the spontaneous fission processes were estimated through compound nucleus excitation energy for atomic number (Z) = 104, 116 and 124 for the first time.
6. A novel Glancing Angle Deposition (GLAD) thin film process has been established to develop multilayer-equivalent high performance broad-band antireflection coatings and devices for high power laser applications in the visible wavelength regimes.

BARC has continued the pioneering work in the field of application of radioisotopes.

1. The first of its kind Radiation Technology based 100 tons/day sewage sludge hygienisation facility is coming up at Ahmedabad. About 60% work has been completed and the plant is expected to be operational by October 2017. This would contribute to the Swachh Bharat Abhiyan and help making cleaner and healthier India.
2. Support to the Indian industry was continued using detailed radiotracer investigations in detecting leakage in high pressure heat exchanger systems at M/s IOCL, Panipat Refinery, Haryana successfully, resulting in substantial economic benefits.
3. Polyurethane based foam modified through gamma radiation grafting technique has been developed which can separate oil/water from layered as well as from emulsified oil/water mixture. The material has promising applications for oil spill cleaning from water, purification of crude oil, emulsified waste water produced in industry and daily life. The material is scalable, mechanically flexible, extensively reusable and economic.

During this period, it was possible for us to develop and transfer many new technologies for societal applications.

1. A Bio-degradable oxocatalyzed polyolefin food packaging film was developed in collaboration with Institute of Chemical Technology, Mumbai. On disposal of these films in the open landfills, in presence of humidity and sunlight, the catalyst develops persistent oxidative radicals, which degrade the polymeric chains. The polymer waste degrades completely within a period of 6-8 months without release of any toxic gases or any residue. The films developed using electron Beam/Gamma irradiation has improved mechanical and barrier properties. It is nontoxic, nonhazardous and safe when in long-term contact with food. The technology is currently being transferred to industry.
2. A bio-pesticide formulation has been developed to kill mosquito larval population in water pools. Its efficacy has been tested under field conditions in different cities of India. The material is non-toxic to human population.
3. A simple and low cost method based on an innovative chemical agent is developed for removal of fluoride from contaminated ground water. In partnership with a private firm, the method has been successfully tested in 10 different villages of Madhya Pradesh.
4. Technology of turmeric based neutraceutical was transferred to a private firm for commercial production.
5. A simple, low cost and portable kit has been developed for detection of chromium in drinking water. This kit provides a much needed method for field detection of carcinogenic chromium (VI) in ground water particularly around the Ganga belt. Technology has been transferred to a private firm for implementation.
6. Indigenous development of dual energy X-ray baggage scanning system using the in-house developed photodetectors has been completed under collaboration with Bharat Electronics Limited. The significance of this development rests on the fact that for the first time in India, pixalated X-ray detectors, which are the most critical part of XBIS are designed and made in India.
7. Technology of polyamide based sea water desalting membrane capable of giving 99% salt rejection with sea water has been developed and transferred to a private firm. Production of commercial size membrane modules based on this technology has been started. This is the first time in India that the sea water desalting membrane and module have been made using indigenous technology.
8. We have commissioned and fine-tuned the Multi-effect Distillation-Thermal Vapour Compression (MED-TVC) technology by commissioning 240m^3/day seawater thermal desalination plant.

Significant contributions have been made in the field of Robotics and Remotization during the last one year.

1. A semi-automated staircase climbing trolley has been designed and developed for material transfer through staircase, upto payload of about 70 Kgs, with single person without any other assistance. This is aimed at providing a low cost solution for taking patients/disabled persons through staircase.
2. A high precision portable surgical coordinate measuring mechanism has been developed for neuro-registration and neuro-navigation. A six-degree of freedom parallel robot for robot based neurosurgery has also been developed. The systems have been function tested in the laboratory. These are ready for clinical trials in the Hospitals. As against commercially available servo-controlled robotic surgical tools, these novel parallel type architecture based robotic tools are first-of-its kind and provide low-cost surgical solution in the Healthcare.

3. As you are aware, BARC has developed the cobalt teletherapy machine Bhabhatron. There has been a continuous effort in improving the performance of 'BHABHATRON' in terms of dose conformity. Towards this, Multi-Leaf-Collimator (MLC) has been designed, developed and integrated with one of the BHABHATRON unit at ACTREC, Mumbai. Its performance evaluation has been successfully completed. It has shown better dose conformity to irregular tumor boundaries, leading to its superior clinical performance. Test reports have been submitted to AERB and regulatory approval is expected shortly.

We have continued to support our space programme in different areas.

1. The indigenous development of Servo controller and 3 axis drives for the 4.6 m Ship-borne terminal has been carried-out by BARC and ECIL in the framework of a contract by ISTRAC/ ISRO on ECIL. The unit is undergoing integration, functional and qualification tests on an indigenously developed single axis ship motion simulator.
2. A Collimator housing assembly and its supporting platform for Neutron radiography facility have been designed, manufactured and supplied to VSSC, Trivandrum under a MoU. The system has been successfully installed at VSSC.

Let me bring out some of the recent achievements in Environmental Monitoring and Radiation Safety.

1. Special monitoring systems like Portable Spectrometer were developed for 35th Indian Scientific Expedition to Antarctica by BARC team jointly with National Centre for Antarctic and Ocean Research (NCAOR), Goa. In addition to these, monitoring system under Indian Environmental Radiation Monitoring Network (IERMON) was also established at 'BHARATI' station and used for environmental radiation monitoring as well as detection and assessment of Thorium in certain locations.
2. A head and Neck phantom has been developed for dosimetry audit in advanced radiotherapy techniques. It will be useful for testing the accuracy of dose delivered to the target organ in advanced radiotherapy techniques. It represents average human head and neck in shape, proportion and composition. Implementation of dosimetry audit will improve the quality and accuracy of radiotherapy treatment.

Continuous efforts are being made to improve infrastructural facilities in various BARC campuses.

1. Under rain water harvesting program, water treatment plant for utilizing lakes located near PP and at foot of Trombay Hill, has been completed and commissioned leading to capacity augmentation of 35 million litres.

In modern times, computational facilities and networking systems are an integral part of infrastructure. I will mention some of the major enhancements.

1. BARC has developed a new parallel supercomputer 'ANUPAM-AGANYA'. The system has been designed and integrated in-house by using commodity hardware and open source and in-house developed software. The peak performance of the system is 380 Teraflops and the sustained performance is 270 Teraflops.
2. BARC in association with CDAC, Trivandrum has developed Network Management System – PRABANDH which is meant for monitoring and managing large sized networks. This has been successfully deployed in ANUNET, National Knowledge Network, Kerala University Network and NIC Network.

Dear Colleagues,

I have mentioned to you highlights of some of our achievements. The list of achievements is very long and due to constraint of time, I am not able to mention many of them. But I must acknowledge the contribution of all my colleagues in BARC, who have worked very hard towards achieving our goals and objectives.

My special thanks are to Medical Division, Administrative Group, Engineering Services Group, Landscape and Cosmetic Maintenance Section, Fire Services, BARC Security and CISF. I also thank members and office bearers of associations and unions for their support, which made all our achievements possible.

While acknowledging these achievements, I must emphasize that we have plenty of challenges ahead. As you are aware, that under NITI Aayog directive, we need to define our 15 year vision, along with identification of deliverables for 3 and 7 years. Hence, we must clearly define our goals and not shift our focus from achieving the same. I am sure that with the coordinated efforts from all of us in BARC; that is scientists, engineers and administrators; we will be able to rise to the occasion to meet the future challenges in a manner consistent with the expectations and tradition of BARC.

Before concluding, I take this opportunity to announce that the BARC Employee's Family Relief Scheme support to bereaved family is enhanced from Rs.1.5 lakh to Rs.1.6 lakh with effect from 30.10.2016.

Colleagues, on this very special day, let us firmly resolve and rededicate ourselves to continue our pursuit of excellence in the frontier areas of nuclear science and technology for the betterment of the life of our fellow countrymen, as envisaged by our visionary founder Dr. Homi Jehangir Bhabha.

Thank you and Jai hind

Successful Clinical Translation of ^{90}Y-Labeled Hydroxyapatite Particles Prepared Utilizing ^{90}Y Produced in Dhruva Research Reactor

Sudipta Chakraborty, K.V. Vimalnath, A. Rajeswari and Ashutosh Dash
Radiopharmaceuticals Division
H.D. Sarma
Radiation Biology and Health Sciences Division
K. Kamaleshwaran and Ajit Shinto
Nuclear Medicine and PET Services, Kovai Medical Centre and Hospital, Coimbatore - 641014

The prospect of using ^{90}Y produced by (n,γ) reaction route in Dhruva research reactor, Trombay for use in the treatment of arthritis of knee joints was explored. Yttrium-90 produced by thermal neutron irradiation of Yttrium oxide (Y_2O_3) target yielded ^{90}Y with specific activity and radionuclidic purity adequate for formulation of hydroxyapatite particles (HA) based radiation synovectomy agent. An optimized kit formulation strategy was developed for convenient one-step compounding of ^{90}Y labeled hydroxyapatite particles (^{90}Y-HA) those are easily deployable at nuclear medicine hospital radiopharmacy. Subsequent to pre-clinical biological evaluation of ^{90}Y-HA particles, the clinical investigations were performed on patients suffering from chronic arthritis in knee joint by localized administration of 185 MBq ^{90}Y-HA into the diseased joints. Preliminary results demonstrated the therapeutic efficacy of the formulation.

Introduction

Intra-articular administration of biocompatible and biodegradable particulates/colloids radiolabeled with a suitable β^- emitting radionuclide is one of the most promising modalities for the treatment of acute and chronic inflammatory joint disorders [1,2]. Administered radiolabeled particulates are phagocytized by the macrophages of the inflamed synovial membrane and deliver selective radiation dose to the synovium leading to necrosis, fibrosis, sclerosis of the proliferating synovial tissue and ablation of the inflamed synovial membrane [1-4]. Three radionuclides namely, ^{90}Y (^{90}Y-silicate/citrate colloid), ^{186}Re (^{186}Re-sulfur colloid) and ^{169}Er (^{169}Er-citrate colloid) are most widely used for large, medium and small joints, respectively [1,2,5,6]. The prospect of using ^{90}Y is unmatched for the treatment of large inflamed joints owing to its attractive nuclear decay characteristics [Half-life = 64.1 h, $E_{\beta max}$ = 2.28 MeV (maximum tissue range 11 mm), no γ emissions].

Cost effective availability of clinically useful ^{90}Y at hospital radiopharmacy is a major impediment in tapping the huge potential of ^{90}Y-labeled particulates/colloids for the treatment of rheumatoid arthritis. While ^{90}Sr/^{90}Y generator system is the conventional source of no carrier added (NCA) ^{90}Y on demand [7], the unavailability of optimally designed ^{90}Sr/^{90}Y generator that can provide ^{90}Y for direct use as radiopharmaceutical ingredient in commercial scale is a major impediment. Consequently, ^{90}Y suitable for *in vivo* therapeutic applications is not available at an affordable cost worldwide, particularly in the developing countries. Alternatively, ^{90}Y is produced by neutron activation of natural yttrium target (yttrium is mononuclidic in ^{89}Y) in a nuclear research reactor, which yields low specific activity ^{90}Y due to the low neutron absorption cross section (1.28 b) of ^{89}Y [8]. We, at the Radiopharmaceuticals Division, BARC have successfully explored the potential therapeutic utility of low specific activity ^{90}Y produced by (n,γ) route in the treatment of arthritis. This treatment can easily be made available to a large population of patients at an affordable cost in India.

In this article, we describe formulation of ^{90}Y-HA [HA, an inorganic polymer of $Ca_{10}(PO_4)_6(OH)_2$ unit] particles using ^{90}Y produced in a medium flux research reactor (Dhruva), chemical and radiochemical characterization of the radiolabeled preparation, its pre-clinical evaluation in animal model and preliminary clinical investigations in human patients suffering from chronic rheumatoid arthritis of knee joints. Towards achieving successful translation of the product from radiochemistry laboratory to clinic, an effective kit formulation strategy was adapted for its expedient formulation at hospital radiopharmacy.

Production, radiochemical processing and quality control of ^{90}Y

Yttrium-90 was produced by irradiating natural Y_2O_3 (mononuclidic in ^{89}Y) target at a thermal neutron flux of ~1×10^{14} n/cm^2.s for a period of 14 d. Subsequently, target was dissolved in 0.1 M suprapure HCl by gentle warming inside a lead-shielded glove box to obtain [^{90}Y]-YCl_3 solution. Specific

activity of ^{90}Y was 851 ± 111 MBq/mg (23 ± 3 mCi/mg) (n = 6) at the end of irradiation (EOI). The radionuclidic purity of ^{90}Y produced was 99.93±0.03% (n = 6) at EOI, with ^{89}Sr, ^{91}Y, ^{160}Tb and ^{169}Yb being the radionuclidic impurities detected.

Preparation of ^{90}Y labeled HA particles

A kit based approach was evaluated for convenient one-step compounding of ^{90}Y-HA that is easily deployable at nuclear medicine hospital radiopharmacy. HA particles of 1-10 µm size range (**Fig. 1**) were synthesized and characterized in as per procedure reported earlier [9,10]. Kits for radiolabeling with ^{90}Y were prepared based on the optimized parameters from systematic preformulation experiments. HA particles (5.0±0.2 mg) were weighed into each of the several sterile glass vials inside a laminar flow hood. Subsequently, 8.4±0.3 mg sodium bicarbonate were weighed and added into each of the glass vials, mixed with HA particles and sealed. Sterile water for injection (1 mL) was added to kit vial followed by addition of 200 ± 10 MBq of ^{90}Y activity as YCl_3 solution. The contents of the kit vials are mixed thoroughly for 5 min using vortex mixture and set aside for 60 min at room temperature without any further agitation. Subsequently, the supernatant is carefully separated from the precipitated ^{90}Y-HA particulates. The radiolabeled HA particles obtained as precipitate are washed using 1 mL sterile saline to ensure the removal of unlabeled (or loosely held) ^{90}Y activity. Finally, the radiolabeled particulates were suspended in sterile normal saline, autoclaved, used for animal studies and human clinical applications after measurement of ^{90}Y activity content.

The yield of ^{90}Y-HA prepared using kits was found to be 98.5 ± 1.1% (n = 25), while the radiochemical purity of labeled particles subsequent to washing with normal saline was 99.5 ± 0.2% (n = 25). ^{90}Y-HA particles showed excellent *in vitro* stability upto a period of 10 d (>3 half-lives of ^{90}Y) in normal saline at 37 °C. Radiochemical purity of the preparation was found to be retained to the extent of >99% during the entire study period. The yields, radiochemical purity, stability of ^{90}Y-HA formulation prepared utilizing reactor produced ^{90}Y-YCl_3 compares well with the formulation prepared using NCA ^{90}Y from Nordion and HA from Bio-Rad as reported by Renata et al. [11].

Pre-clinical biological studies

The pre-clinical biological evaluation of ^{90}Y-HA particles was studied by carrying out biodistribution and bioluminescence imaging studies in Wistar rats artificially induced with arthritis in one of the knee joints. The results showed retention of > 98% of the injected activity within the joint cavity even after 168 h post-administration (**Fig 2**). Activity

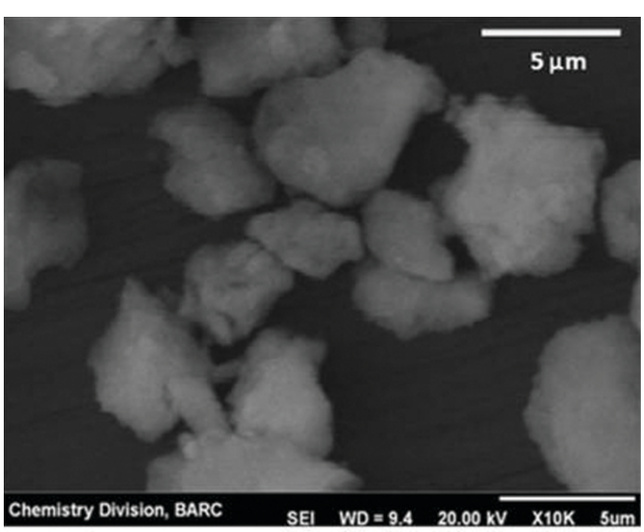

(a)

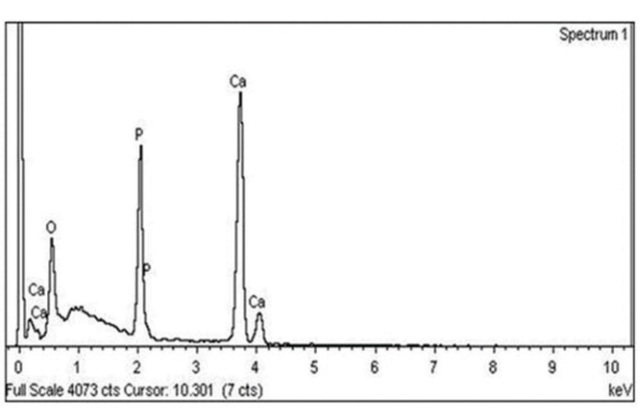

(b)

Fig.1: (a) Scanning electron micrograph (b) ED spectrum of hydroxyapatite microparticles

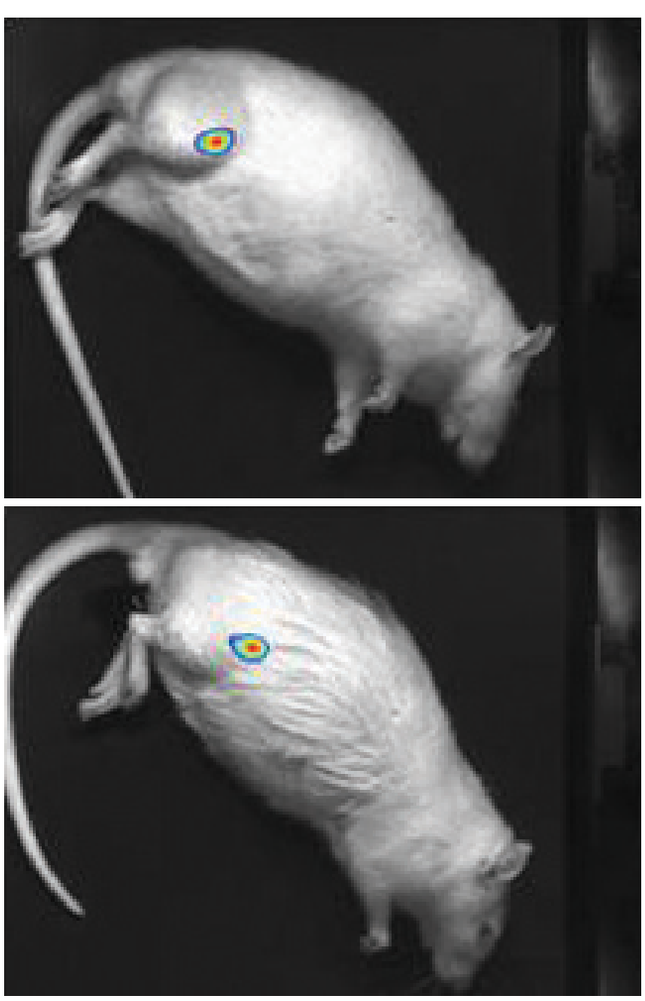

Fig.2: Whole body bioluminescence images of Wistar rats at 72 h (top) and 168 h (bottom) after intra-articular administration of ^{90}Y-HA into the arthritis induced knee joint

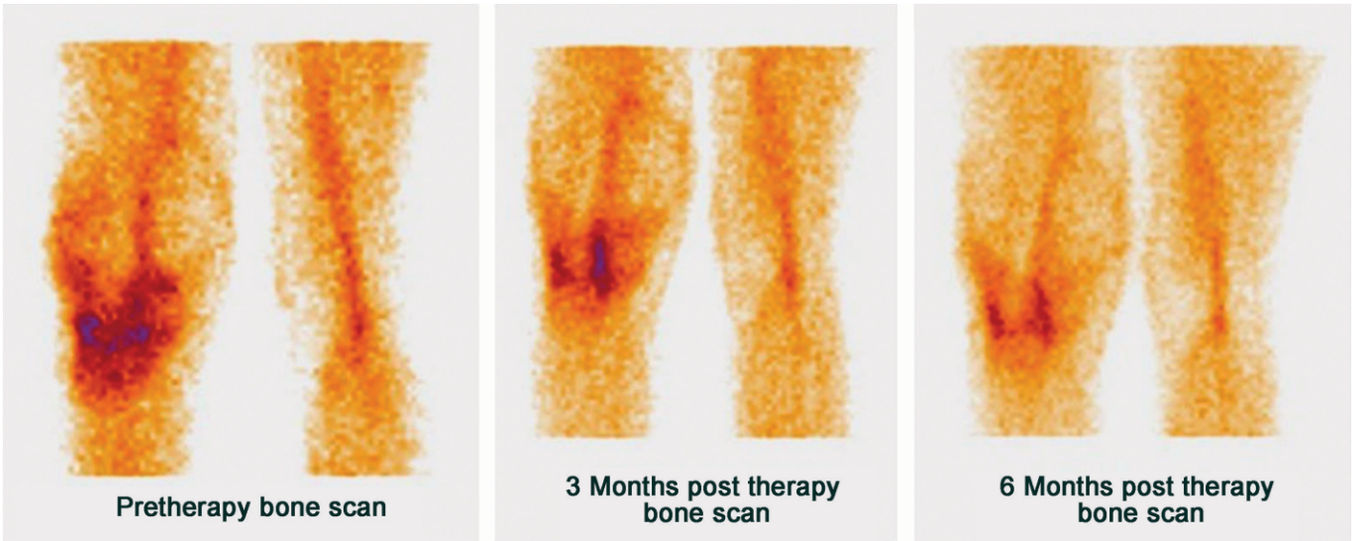

Fig.3: Pre-therapy, 3 months post-therapy and 6 months post-therapy ^{99}Tc-MDP scans of knee joint region of the patient treated with ^{90}Y-HA, clearly demonstrating significant reduction of synovial inflamation as a direct evidence of therapeutic efficacy of ^{90}Y-HA

detected in blood and other major organ/tissue was insignificantly low. The results of biological evaluations obtained by indigenously developed ^{90}Y-HA formulation are comparable to those obtained from NCA ^{90}Y as reported by Renata et al. by Bremsstrahlung scintigrapy of ^{90}Y-HA in Wistar rats [11].

Clinical study

Radiation synovectomy (RSV) using ^{90}Y-HA was performed on five patients with clinically proven rheumatoid arthritis (RA) of knee joints who are suffering from persistent joint pain and lack of mobility despite ongoing pharmacotherapy with anti-inflammatory and analgesic drugs. Dose of ^{90}Y-HA particles (185 MBq) dispersed in 1 mL of sterile, pyrogen free normal saline was administered intra-articularly into each affected joint. The clinical study was approved by the local institutional ethics committee (Reference No. EC/AP/244/07/2013, Registration No ECR/113/INST/TN/2013), and the patients provided written informed consent. Results of the preliminary clinical investigations showed that the administered ^{90}Y-HA activity was retained completely within the knee joint cavity as no leakage of ^{90}Y activity into any other non-target organs were visible in the serial whole body scans recorded upto 7 d post-administration of ^{90}Y-HA. The representative scan of a typical treated knee joint recorded 24 h post-administration of ^{90}Y-HA recorded using Bremsstrahlung radiation from ^{90}Y depicts excellent localization of the radiolabeled particulates in the joint cavity with almost no extra-articular leakage. Assessment of treatment efficacy carried out over a period of six months based on the information from the patients showed substantial improvement in the disease conditions such as, reduction in joint effusion, local pain and improvement in the range of motion. Analysis of RSV treatment outcome at 6 months follow-up was based on the detailed information received from patients, clinical examinations and three phases bone scintigraphy (BS). Treatment outcome was examined in terms of joint pain during exercise, improvement measured with a 100– point visual analog scale (VAS) pain score, before and at 6 months after treatment. Six months after RSV, the VAS improvement from baseline values of the knee pain for the patient was 75 ±15%. A comparison of pre-therapy, 3 months post-therapy and 6 months post-therapy ^{99}Tc-MDP scans of the knee joint region of a patient (**Fig. 3**) clearly demonstrates significant reduction of synovial inflamation as a direct evidence of therapeutic efficacy of ^{90}Y-HA. More the improvement in VAS score, more decrease in blood pooling compared to pretherapy scintigraphic changes were noted. Long-term treatment efficacy based on quantitative data obtained from clinical and pathological examinations are encouraging.

Conclusion

The utility of ^{90}Y obtained from neutron activation production route for the formulation of clinical doses of ^{90}Y-HA particles using ready-to-use single vial kits of HA particles at the hospital radiopharmacy set up is successfully developed and demonstrated. The single-vial kit, provided a convenient and reproducible method for facile preparation of ^{90}Y-HA particles (200 ± 10 MBq) with high yield (>98%) and radiochemical purity (>99%) in a clinical setting. Preliminary clinical studies demonstrate the effectiveness of ^{90}Y-HA in terms of pain control, functional improvement and prevention of disease progression in rheumatoid arthritis patients. Although radiation synovectomy (RSV) with ^{90}Y based radiopharmaceuticals have been used extensively in Europe for the past 25 years to treat rheumatoid arthritis in the knee joint [12], it has generated only modest clinical interest in India till date. The comprehensive and systematic study from radiochemistry laboratory to nuclear medicine clinic demonstrates a potential therapeutic utility of indigenous (n,γ) produced ^{90}Y in India.

Acknowledgements

The authors sincerely thank Dr. B.S. Tomar, Director, RC&I Group for his keen support. The authors also gratefully acknowledge Dr. S.V. Thakare and Shri K.C. Jagadeesan of Radiopharmaceuticals Division and staff members of Reactor Operation Division, BARC, for arranging the irradiation of Y_2O_3 targets in Dhruva research reactor.

References

1. Schneider P, Farahati J, Reiners C. "Radiosynovectomy in rheumatology, orthopedics, and hemophilia". *J Nucl Med*, 46, (2005): 48S-54S.
2. Deutsch E, Brodack JW, Deutsch KF. "Radiation synovectomy revisited". *Eur J Nucl Med*, 20, (1993): 1113-1127.
3. Mödder G. Radiation Synovectomy. In: Biersack HJ, Freeman LM, editors. *Clinical Nuclear Medicine. Springer Verlag, Berlin Heidelberg*, *2007*, pp. 512–518.
4. Wang SJ, Lin WY, Chen MN, Chen JT, Ho WL, Hsieh BT, Huang H, Shen LH, Ting G, Knapp FF Jr. "Histologic study of effects of radiation synovectomy with Rhenium-188 microsphere". *Nucl Med Biol*, 28, (2001): 727-732.
5. Clunie G, Fisher M. "EANM procedure guidelines for radiosynovectomy". *Eur J Nucl Med Mol Imaging*, 30, (2003): BP12-BP16.
6. van der Zant FM, Boer RO, Moolenberg JD, Jahangier ZN, Bijlsma JWJ, Jacobs JWG. "Radiation synovectomy with ^{90}Yttrium, ^{186}Rhenium and ^{169}Erbium: a systematic literature review and meta-analysis". *Clin Expt Rheumatol*, 27, (2009): 130-139.
7. Chakravarty R, Dash A, Pillai MRA. "Availability of Yttrium-90 from Strontium-90: a nuclear medicine perspective". *Cancer Biother Radiopharm* 27, (2012): 621-641.
8. *Atlas of neutron capture cross sections. IAEA Nuclear Data Section, Vienna, Austria, 1997.*
9. Unni PR, Chaudhari PR, Venkatesh M, Ramamoorthy N, Pillai MRA. "Prepration and bioevaluation of ^{166}Ho labeled hydroxyapatite (HA) particles for radiosynovectomy". *Nucl Med Biol*, 29, (2002): 199-209.
10. Rajeswari A, Vimalnath KV, Sarma HD, Shetty P, Mohammed SK, Nuwad J, Chakraborty S, Dash A. "Hydroxyapatite microparticles labeled with ^{32}P – a promising option in the radiation synovectomy of inflamed joints". *Appl Radiat Isotope*, 116, (2016): 85-91.
11. Couto RM, Barboza de MF, Souza de AA, Muramoto E, Mengatti J and Araújo de EB. "In vivo comparative study of hydroxyapatite labeled with different radioisotopes: evaluation of the scintigraphic images". Cell. Mol. Biol. 56 (2010): 6-11.
12. Spooren PF, Rasker JJ, Arens RP. "Synovectomy of the knee with ^{90}Y". Eur J Nucl Med. 10 (1985): 441-445.

Production of ^{99}Mo-^{99m}Tc Medical Isotopes using Accelerator as an Alternative Route

H. Naik
Radiochemistry Division
S.V. Suryanarayana
Nuclear Physics Division
A. Gopalakrishna
Medical Cyclotron Facility, Radiation medicine Centre, Mumbai 400012, India
G.N. Kim
Department of Physics, Kyungpook National University, Daegu 702-701, Republic of Korea
Roberto Capote Noy
Department of Nuclear Sciences and Applications, IAEA, Vienna-1001400, Austria

The ^{99}Mo radio-nuclides were produced in the ^{100}Mo(γ, n) reaction by using photon beams obtained from the electron LINAC of 10 MeV at Electron Beam Centre (EBC), Kharghar, Navi-Mumbai, 20 MeV at Helmholtz-Zentrum Dresden-Rossendorf (HZDR), Dresden, Germany and 100 MeV at Pohang Accelerator Laboratory (PAL), Pohang, South Korea. The ^{99}Mo isotopes were also produced in the ^{238}U(γ, f) reaction using the 8 MeV microtron at Mangalgangotri University, Mangalore, Karnataka, India as well as the electron LINAC of 10 MeV at EBC, Kharghar and 35 MeV at CEA, Saclay, France. The ^{99m}Tc nuclei are produced in a generator from its parent ^{99}Mo decay. The daughter product ^{99m}Tc is radio-chemically separated from its parent activity ^{99}Mo produced in the ^{100}Mo(γ, n) reaction to determine the chemical yield. The activities of ^{99}Mo and ^{99m}Tc were analyzed by a γ-ray spectrometric technique using an HPGe detector. From the detected γ-rays activities of 739.8 keV and 140.5 keV, the amount of ^{99}Mo and ^{99m}Tc produced were determined. The production of ^{99}Mo activity in the ^{238}U(γ, f) and ^{100}Mo(γ, n) reactions is an alternate approach. Thus its viability and practicality has been discussed in comparison to the production through ^{235,238}U(n, f) and ^{98}Mo(n, γ) reactions for circumventing the need for a reactor. An estimate has been also arrived based on the experimental data to fulfil the requirement of DOE, USA.

Introduction

The neutron induced fission of uranium was discovered in 1939 by Hahn and Strassmann [1]. Subsequent to this, photon induced fission of uranium and thorium was discovered in 1941 by Haxby et al. [2]. Over the years, experimental and theoretical work has been carried out all over the world in exhaustive way for the neutron induced fission/reaction studies but in a limited way for the photon induced fission/reaction. The neutron-and photon-induced fission/reaction cross-sections [3,4] of various elements are important for different applications such as the design of radiation shielding, the calculation of absorbed dose in the human body during radiotherapy, in the physics and technology of fusion/fission reactors, nuclear waste transmutation, astrophysical nucleo-synthesis and for the radioactive isotopes productions.

In neutron, photon and charged particle induced fission and reactions of various elements; about 3000 radioactive isotopes are produced. Among these, 1000 are employed for commercial applications in academic, industrial and medical field [5-10]. About 140 radioisotopes are used worldwide in medical field [8, 9], which involves diagnosis (both in vivo and vitro), therapeutic and preventive applications [5, 8]. Only 10 isotopes are used in 90% of all in vivo nuclear medicine procedures performed per year [6, 7]. About 70,000 diagnostic images are taken each day, worldwide. Among the medical radioisotopes, ^{99m}Tc is utilized in 80% of all non-invasive nuclear diagnostic imaging [11-16] of various organs all over the world. The ^{99m}Tc has a half-life of 6.01 hours [17, 18] that decays to the much long-lived ^{99g}Tc by emitting a 140.5 keV gamma ray. It can be bound into a variety of special molecules that target specific parts of the body when ingested or injected [15, 16]. Its location within the body can be pinpointed by detecting the 140.5 keV gamma ray in single photon emission computed tomography (SPECT) imaging. Thus the radionuclide ^{99m}Tc is very important from the medical application point of view [5-16]. The ^{99m}Tc is usually produced by milking out in a generator from the decay of parent ^{99}Mo, which has a half-life of 65.94 hours [17, 18].

In a research reactor, high specific activity of ^{99}Mo is produced in the ^{235}U(n, f)^{99}Mo reaction. About 90% of ^{99}Mo used in the world is produced in reactor in the ^{235}U(n_{th}, f) reaction using highly enriched (93%) uranium (HEU) and 10% from ^{98}Mo(n_{th}, γ) reaction. Nearly all the global supply of ^{99}Mo is produced at just five reactors. These are (a) the high flux reactor (HFR) in Petten, the Netherlands, (b) BR-2 in Mol, Belgium, (c) Osiris in Saclay, France, (d) the National Research Universal (NRU) in Chalk River, Canada, North America and (e) Safari-1 in Pelindaba, South Africa. All these reactors are over 40 years old [13, 14] and produced

^{99}Mo–^{99m}Tc from thermal neutron induced fission of highly (93 %) enriched ^{235}U (HEU), which is of weapons grade. The HEU is very expensive and have restriction by IAEA for ^{99}Mo production. In order to avoid HEU, the activity of ^{99}Mo is being produced using low enriched uranium (LEU). As for example OPAL in Australia is producing ^{99}Mo from LEU targets. Similarly, SAFRI-I in South-Africa has also changed the enriched ^{235}U to <20 %. In addition to these major producers, the National Atomic Energy Commission (CNEA) of Argentina has been producing ^{99}Mo since 2002 using LEU targets. However, production of ^{99}Mo from ^{235}U(n_{th}, f) using HEU or LEU is not favourable with respect to the cost, safety, licensing, radioactive waste and complications to make a reactor.

Production of ^{99}Mo–^{99m}Tc can be done from the fast neutron induced fission of ^{238}U using the fast reactor or accelerated driven sub-critical system (ADSs). However, with fast neutrons, the ^{238}U(n, f) reaction has low fission cross-section [3] and is so far not used, whereas high neutron flux spallation source in ADSs is not yet developed. In the ^{235,238}U(n, f)^{99}Mo reaction, many long-lived radioactive waste with total activity of fifty times the activity of ^{99}Mo are formed [19, 20]. To avoid the radioactive waste, required ^{99}Mo activity can be obtained from the ^{98}Mo(n_{th}, γ) reaction by using enriched ^{98}Mo target and high flux reactor. It is also possible to produce the activity of ^{99}Mo in the ^{100}Mo(n, 2n)^{99}Mo reaction [21, 22]. In the high-energy neutron-induced reaction, other reaction products are also produced along with ^{99}Mo. The activity of ^{99}Mo and its daughter product ^{99m}Tc can be produced in the ^{100}Mo(p, pn) and ^{100}Mo(p, 2n) reactions [23–30]. For proton beam, these reactions have some threshold with low reaction cross-sections. At high proton energies, other reaction channels such as (p, n), (p, a), (p, np) and (p, na) also open up resulting in many reaction products from the ^{100}Mo targets. Besides this, in the proton-induced reactions of ^{nat}Mo, many radioactive products with high specific activities are produced. Thus ^{nat}Mo is used as a target for the production of medical radio-isotopes such as ^{99}Mo-^{99m}Tc, ^{96r}Tc, ^{94m}Tc by using different nuclear reactions. This is because ^{nat}Mo has the isotopic composition of ^{92}Mo (14.84%), ^{94}Mo (9.25%), ^{95}Mo (15.92%), ^{96}Mo (16.68%), ^{97}Mo (9.55%), ^{98}Mo (24.13%) and ^{100}Mo (9.63%), respectively. Further, to improve the production yield of ^{99}Mo in the ^{238}U(p, f) and ^{100}Mo(p, 2n) reactions, particle accelerators [23-30] should have high proton current. In the ^{100}Mo(p, 2n) reaction, the biggest disadvantage is that the final product ^{99m}Tc ($T_{1/2}$ = 6.01 h) is directly produced. Thus, its usefulness would be hampered if it is needed to be shipped over great distance to the end users.

As a probable alternative to all the above, ^{238}U(γ, f) reaction using accelerator was suggested by Ruth [13]. He noted that the quantity ^{99}Mo in the ^{238}U(γ, f) reaction is several orders of magnitude less than ^{235}U(n, f) route. Besides this, the production of ^{99}Mo in the ^{238}U(γ, f) reaction is significantly higher compared to charged particles [12, 24] or neutrons induced fission of ^{238}U, in spite of relatively lower specific activity (3.7 x10^{10} Bq/g) of produced isotopes in the former than the latter. Ruth [13] has noted that the quantity of ^{99}Mo in the ^{238}U(γ, f) reaction can be sufficiently enhanced by using a higher photon flux, which is possible by increasing the electron current. The production of ^{99}Mo–^{99m}Tc based on distributed electron accelerators and thermal separation was mentioned by Bennett et al. [31] based on the ^{100}Mo(γ, n)^{99}Mo reaction. Similarly, others [32–35] have also mentioned about the production of ^{99}Mo in the photo-nuclear reaction of ^{nat}Mo and enriched ^{100}Mo by using electron linac. Since the ^{nat}Mo have many isotopes, their (γ, x) reactions at higher photon energy produce $^{91-88}$Mo and other radioactive nuclides such as $^{90-97}$Nb and $^{86-89}$Zr besides ^{99}Mo [36, 37]. The mono-energetic photon with sufficient flux is difficult to obtain. Thus production of useable activity of ^{99}Mo in the ^{100}Mo(γ, n) reaction with mono-energetic photon is a difficult task. Nowadays most of the photo-nuclear reactions studies have been made by the use of bremsstrahlung from electron accelerators. Owing to the development of accelerator technology, there is the possibility of ^{99}Mo production in the ^{100}Mo(γ, n) reaction as an alternative to the ^{98}Mo(n_{th}, γ) reaction. This is because the ^{100}Mo(γ, n)^{99}Mo reaction has higher cross-section of 0.1523 barns at the photon energy of 14.56 MeV [38] compared to the ^{98}Mo(n_{th}, γ)^{99}Mo reaction cross-section of 0.130 barns [3]. In ^{nat}Mo, the isotopic abundance of ^{100}Mo is 9.63%, whereas for ^{98}Mo, it is 24.13%. The ^{100}Mo(γ, n)^{99}Mo and ^{nat}Mo(γ, xn)$^{88-91,99}$Mo reaction cross-sections at the bremsstrahlung end-point energies of 12–16 and 45–70 MeV have been determined by us using activation and off-line γ-ray spectrometry technique. [39-41]. Similarly, the fission yield of ^{99}Mo in the ^{238}U(γ, f) reactions at different bremsstrahlung end-point energies has been shown by us [42-44] and others [45-52]. The production of ^{99}Mo activity in the ^{100}Mo(γ, n), ^{nat}Mo(γ, xn) and ^{238}U(γ, f) reactions at different bremsstrahlung end-point energies has been shown by us [53] and others [9, 13]. Similarly, the radiochemical separation of the ^{99}Mo in the ^{100}Mo(γ, n) and ^{nat}Mo(γ, xn) reaction at the bremsstrahlun induced reaction has been also done by us [54]. The experiment carried out using ^{238}U(γ, f) and ^{100}Mo(γ, n) reactions [53-55] are alternative to ^{235}U(n, f) and ^{98}Mo(n, γ) reactions for the preparation of ^{99}Mo, which has been discussed in detail in the present article.

Experimental Details

The production of ^{99}Mo activity [53-55] and its fission yields [42-44] in the ^{238}U(γ, f) reaction was carried out with the bremsstrahlung end-point energies of 8 MeV using microtron at Mangalgangotri University, Mangalore, Karnataka, India; with 10 MeV using the electron LINAC at EBC, Kharghar, Navi-Mumbai, India as well as with 11.5, 13.4, 15.0 and 17.3 MeV using the Spectrometer Arrangement for Photon Induced Reactions (SAPHIR) facility at CEA, Saclay, France.

On the other hand, the production of ^{99}Mo activity, its chemical yield [53-55] and cross-section [39-41] from the ^{100}Mo(γ, n) reaction using electron LINAC was carried out with the bremsstrahlung end-point energies of 10 MeV at EBC, Kharghar, Navi-Mumbai, India; with 12, 14 and 16 MeV at HZDR, Dresden, Germany as well as with the 45, 50, 55, 60 and 70 MeV at PAL, Pohang, South Korea. Besides these, the chemical yield of ^{99m}Tc from ^{99}Mo based on the ^{100}Mo(γ, n) reaction was also determined by us using the 10MeV and 15 MeV electron LINACs of BARC and SAMIR at EBC, Kharghar, Navi-Mumbai.

Production of photon beam as bremsstrahlung

In the above mentioned electron accelerators, the photon beam as bremsstrahlung was generated by impinging the electron beam from electron accelerators on different high-Z target materials under different conditions. The electron beam specifications of the electron accelerators used are given in Table 1.

In the microtron centre at Mangalore, the bremsstrahlung beam was produced by impinging 8 MeV pulsed electron beam on 0.188 cm thick Tantalum [Ta] target [44]. At EBC, Kharghar, the bremsstrahlung beam was produced by impinging 10 MeV pulsed electron beam on a 1 mm thick tantalum metal foil [39, 42]. In both the cases the Ta targets, which act as electron to photon converter were located at a distance of 3 cm from the beam exit window and the samples were kept at a distance of 10 cm from the Ta target. The arrangement used for the bremsstrahlung irradiation is shown in Fig. 1.

In the 20-MeV electron LINAC ELBE at HZDR, Dresden, Germany the bremsstrahlung end-point energy of 12-16 MeV was generated by impinging the electron beam on a solid graphite beam dump [40, 41].. In the 35-MeV electron LINAC, SAPHIR at CEA Saclay, France [43], the bremsstrahlung end-point energy of 11.5-17.3 MeV was produced by impinging a pulsed electron beam on a light water cooled cylindrical tungsten target of 5 cm diameter and 5 mm thickness [43]. In the 100-MeV electron LINAC at PAL, Pohang, South Korea, the bremsstrahlung end-point energy of 45-70 MeV was generated when a pulsed electron beam hit thin tungsten (W) metal foil with a size of 10.0 cm×10.0 cm and a thickness of 0.1 mm. The W target was placed on a suitable stand at 18.0 cm from the electron beam exit window [40, 41]. Typical bremsstrahlung spectra generated using GEANT4 code [56] for the above arrangement is given in Fig. 2.

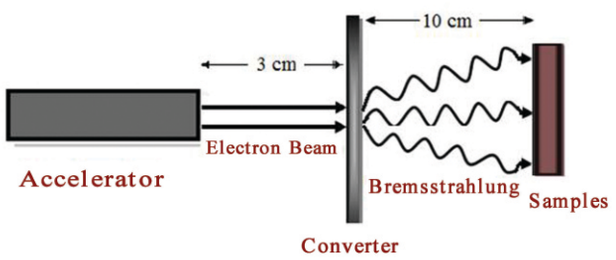

Fig.1: Schematic diagram showing the arrangement for the production of bremsstrahlung

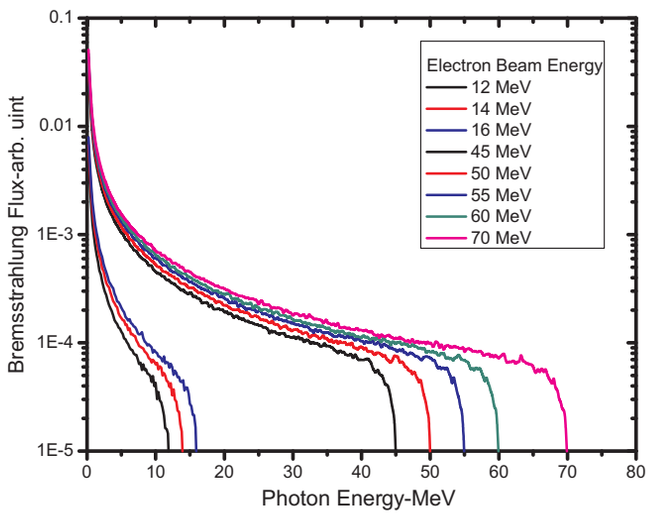

Fig. 2: Photon flux in arbitrary unit as a function of photon energy calculated using GEANT4 code

Table 1. Electron beam specifications of the electron accelerators used from India, Germany, France and South Korea.

Beam specification	Microtron at Mangaluru, Karnataka, India	Electron LINAC at Kharghar, Navi-Mumbai, India EBC and SAMIR		Electron LINAC (ELBE) at HZDR, Dresden, Germany	Electron LINAC (SAPHIR) at CEA, Saclay, France	Electron LINAC (PAL) at Pohang South Korea
Beam Energy	8 MeV	10 MeV	15 MeV	12-16 MeV	11.5-17.3 MeV	45-70 MeV
Peak Beam current	50 mA	100-200 mA	65 mA	42.7 mA	100 mA	100 (10-50) mA
Pulse width	2.5 μs	10 μs	6 μs	10 ps	2.5 μs	1-2 (1.5) μs
Pulse repetition rate	250 Hz	300-400 Hz	20-150 Hz	13 MHZ	25 Hz	10-12 (3.75) Hz
Average Beam current	0.3 mA	0.3-0.8 mA	7.8 μA	555 μA	6.25 μA	1-2 (0.056-0.28) µA

Sample preparation, irradiation and gamma-ray counting

In the photo-fission work, for the production of ^{99}Mo activity, ^{nat}U-metal foil of thickness 2.7 cm^2 and mass 0.2608 gm was wrapped with 0.025 mm thick Al foil and irradiated for 3-4 hours with the bremsstrahlung end-point energy of 8 MeV using the microtron facility at Mangalore, India [44]. For 10 MeV, 0.2414 gm of ^{nat}U-metal foil with an area of 2.5 cm^2 was wrapped with Al foil and irradiated for 4-5 h using the electron LINAC at EBC, Kharghar, India [42]. Similarly, at 11.5-17.3 MeV, 5.6 gm of ^{nat}U-metal rod of diameter 2.74 mm and length 5 mm weighing 5.6 gm was mounted inside a pneumatic rabbit holder and irradiated for 30 minutes using the pneumatic carrier facility of SAPHIR, CEA, Saclay, France [43].

In the photo-nuclear reaction work, 119.1-393.1 mg of ^{nat}Mo metal foil (area 0.196 cm^2) was wrapped with 0.025 mm thick Al foil and placed at a distance of 10 cm from the Ta target. The samples were irradiated for 3-4 h with bremsstrahlung end-point energy of 10 MeV [39, 53] using the electron LINAC at EBC, Kharghar, India. For the 12-16 MeV [40, 41], three ^{nat}Mo metal foil of about 54.8-88.04 mg weight, 0.1 mm thick and 0.6-0.8 cm^2 area was wrapped with 0.025 mm thick Al foil. The Al wrapped metal samples were kept separately inside three different capsules made of polypropylene and loaded on a sample holder. They were sent to the irradiation site one at a time using pneumatic carrier rabbit facility of ELBE at HZDR, Germany [40, 41]. The area directly behind the electron beam dump was used as a site for high flux irradiations. The samples were irradiated for 8.367-10.45 hours. For 45-70 MeV, five ^{nat}Mo metal samples of about 109.3-119.2 mg of ^{nat}Mo with 1.0 mm^2 area was wrapped with 0.025 mm thick Al foil. The Al wrapped sample was placed at a distance of 12 cm from the tungsten target and was positioned at zero degree with respect to the direction of the electron beam [40, 41]. The samples were irradiated for 20–30 min with the bremsstrahlung produced by bombarding the 45–70 MeV electrons on the tungsten metal foil in the electron LINAC at PAL, Pohang, South Korea.

The Al wrapped irradiated samples of ^{nat}Mo and ^{nat}U from their irradiation site were manually transported for the bremsstrahlung end-point energies of 8, 10 and 45-70 MeV and by using pneumatic transport technique for the 11.5-17.3 and 12-16 MeV. The irradiated samples of ^{nat}Mo and ^{nat}U wrapped with Al were analysed for the activities of ^{99}Mo and fission products by off-line γ-ray spectrometric technique using an energy and efficiency calibrated HPGe detector coupled to a PC based 4-16K channel analyzer. The resolution of the detector system was 2.0 keV full width at half maximum (FWHM) at the 1332.0 keV γ-line of ^{60}Co. A typical gamma ray spectrum of irradiated ^{nat}Mo and ^{238}U samples wrapped with Al are shown in Figs. 3 and 4, respectively.

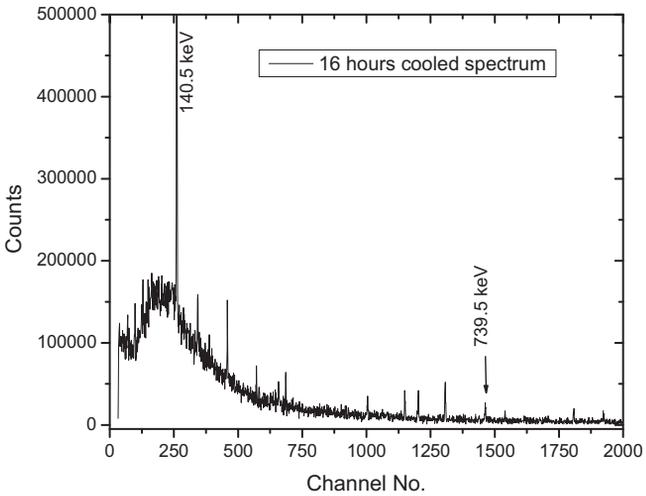

Fig. 3: Typical γ-ray spectrum of an irradiated ^{nat}Mo showing the γ-lines of ^{99}Mo

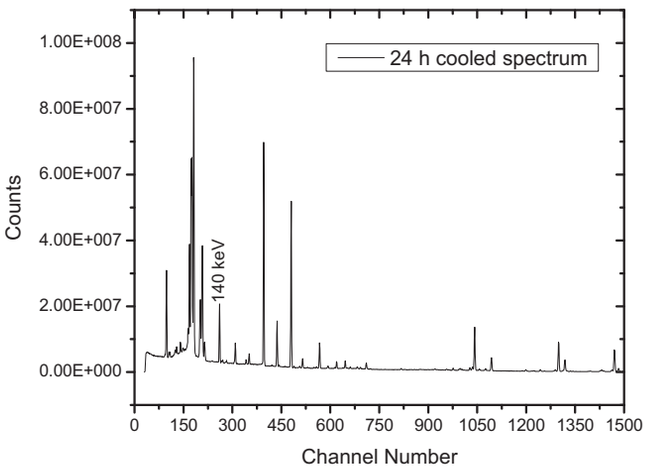

Fig. 4. Gamma ray spectrum of fission products in the ^{nat}U(γ, f) reaction

Radiochemical separation of ^{99m}Tc from ^{99}Mo generator

Production of "^{99}Mo from the fission of uranium involves a complex and expensive technology. Further large quantities of highly toxic radioactive wastes are produced in the fission process. The fission route is therefore not practicable for most developing countries. Fission product, ^{99}Mo is now routinely produced only in a few large production centres in the world. In view of this an alternative technology for the production of ^{99m}Tc from ^{99}Mo by non fission routes such as ^{100}Mo(γ, n) reaction is preferable [31-41]. In conventional way, the enriched ^{100}Mo metal or its oxide is first irradiated with bremsstrahlung radiation. After irradiation, the molybdenum target can be dissolved in nitric acid or hydrogen peroxide to form molybdenum oxide (MoO_3). Different separation techniques can be used to separate the technetium from the molybdenum oxide. One of this is the sublimation process, in which the technetium and molybdenum oxide can be separated based on the different vapour pressure. However, most of the common techniques use columns that selectively bind either the technetium or molybdenum present in solution. In the most technetium generator, the Mo is retained on alumina column and the technetium washed off. This is

good where the specific activity of ^{99}Mo is quite high as in the case of $^{235}U(n_{th}, f)$ reaction [57]. However, in case of $^{nat}U(\gamma, f)$ reaction and primarily in the $^{nat}Mo(\gamma, n)$ or $^{100}Mo(\gamma, n)$ reactions, the specific activity of ^{99}Mo is two orders of magnitude smaller. In such cases, the development of fully Automated Radionuclide Separation (ARSII) developed by North Star [58] is suitable. The ARSII reverse the approach of the conventional generator. In ARSII, the column selectively retains the technetium as the parent solution passes over it. Thus, the technetium can be extracted from relatively large volume of parent solution. Once the column is cleared from the parent solution, a separate saline rinse of the column and removes the technetium as sodium per-technetate ($NaTcO_4$). This fulfils the same specifications as the solution obtained from a conventional generator.

We have developed a special radiochemical technique [44] to separate ^{99m}Tc from ^{99}Mo generator and compared with the conventional separation technique. First ^{99}Mo-^{99m}Tc was produced from the $^{100}Mo(\gamma, n)$ reaction of the natural molybdenum trioxide (MoO_3) and zirconium molybdate gel. For this purpose different packets of sample of about 0.23 to 0.6 g of molybdenum trioxide powder and 0.98 to 6 g of zirconium molybdate gel were wrapped separately with 0.025 mm thick Al foil. They were combinely wrapped with additional Al foil of same thickness. In the electron LINAC of EBC, BARC, the target assembly was irradiated for 2–3 hours with the bremsstrahlung end-point energy of 10 MeV. In the case of electron LINAC of EBC, SAMIR, the target assembly was irradiated only for 30 to 45 min with the bremsstrahlung end-point energy of 15 MeV. The irradiated targets from both the electron LINAC were bought to Radiochemistry Division lab after waiting time of 0.5 to1 hours. In two days of cooling time, the ^{99m}Tc reached in equilibrium with ^{99}Mo and thus decay with the half-life of ^{99}Mo. After the equilibrium, ^{99m}Tc was separated as $NaTcO_4$ from the irradiated samples using two different chemical procedures to examine the chemical yield. The ^{99m}Tc from the irradiated molybdenum trioxide was separated by conventional solvent extraction using methyl ethyl ketone (MEK). On the other hand, ^{99m}Tc from the irradiated zirconium molybdate gel was separated by simple column elution with saline/acetone solution. The separated $Na[^{99m}Tc]TcO_4$ from the ZrMo gel has the ^{99}Mo breakthrough of $< 10^{-4}$ %, radiochemical purity >99% as well as chemical impurities of Al, Mo and Zr <10 ppm. The activity of ^{99}Mo and ^{99m}Tc in the undissolved samples and in the separated samples were estimated by off-line γ-ray spectrometric technique.

Calculation and results

The photo-peak areas (A_{obs}) of the 140.5 keV and 739.8 keV γ-lines of the fission or reaction product ^{99}Mo from the $^{100}Mo(\gamma, n)$ and $^{238}U(\gamma, f)$ reactions were calculated by subtracting the linear Compton background. The observed γ-ray activity (A_{obs}) of the ^{99}Mo produced from the ^{100}Mo (γ, n) and $^{238}U(\gamma, f)$ reactions was used for its activity determination.

Calculation of ^{99}Mo activity from the experimentally obtained photo-peak area

In the $^{238}U(\gamma, f)$ and $^{100}Mo(\gamma, n)$ reactions, the observed γ-ray activity (A_{obs}) is related to the photo-fission/reaction cross-section (σ_F/σ_R) of ^{99}Mo [42-44] as

$$A_{obs}(CL/LT) = N\sigma_F\Phi Ya\,\varepsilon\,(1-e^{-\lambda t})\,e^{-\lambda T}\,(1-e^{-\lambda CL})/\lambda \quad (1)$$

$$A_{obs}(CL/LT) = N\sigma_R\Phi a\,\varepsilon\,(1-e^{-\lambda t})\,e^{-\lambda T}\,(1-e^{-\lambda CL})/\lambda \quad (2)$$

where N is the number of target atoms, Φ is the photon flux. 't' and T are the irradiation and cooling time. CL and LT are the real and live time respectively. 'λ' is the decay constant of the isotope of interest, which is ^{99}Mo in the present case. 'a' is the abundance or branching intensity of the chosen γ-rays of the fission/reaction product (^{99}Mo-^{99m}Tc). 'ε' is the efficiency of the detection system at a fixed geometry of the γ-lines studied. Y is the cumulative yield of ^{99}Mo in the $^{238}U(\gamma, f)$ reaction [42-52].

The nuclear spectroscopic data such as half-life ($T_{1/2}$) and branching intensity (a) for ^{99}Mo-^{99m}Tc are taken from Refs. [17, 18] and are given in Table 2 along with the threshold energies for the $^{238}U(\gamma, f)$ and $^{100}Mo(\gamma, n)$ reactions.

The efficiency (ε) of the γ-ray energy for the detector system at a fixed geometry was calculated as:

$$\ln\varepsilon = \Sigma\, C_n (\ln E)^n \quad (3)$$

where C_n represents the fitting parameters and E is the γ-ray energy for a ^{152}Eu standard source with various γ-ray energies from 121.8 keV to 1408.0 keV.

Table 2: Nuclear spectroscopic data of ^{99}Mo-^{99m}Tc and the threshold energies for the $^{238}U(\gamma, f)$ and $^{100}Mo(\gamma, n)$ reactions.

Reaction	Threshold energy	Reaction Product	Half-life	Decay mode	Gamma-ray energy in keV	Branching intensity
$^{238}U(\gamma, f)$	4.0 MeV	^{99}Mo	65.976 h	β^- (100 %)	181.07	6.14
					739.8	12.26
		^{99m}Tc	6.0067 h	IT (100 %)	140.5	89.43
$^{100}Mo(\gamma, n)$	8.29 MeV	^{99}Mo	65.976 h	β^- (100 %)	181.07	6.14
					739.8	12.26

The 'ε' value from Eq. (3), 'a' from Refs. [24-27] and the photo-peak areas (A_{obs}) of the 140.5 keV and 739.8 keV γ-lines are related to the disintegration per second (DPS) of ^{99}Mo with the following relation

$$DPS = A_{obs}(CL/LT)/ [e^{-\lambda T} (1 - e^{-\lambda CL}) (LT) (\varepsilon) (a)] \quad (4)$$

The DPS of ^{99}Mo in the ^{238}U(γ, f) and ^{100}Mo(γ, n) reactions for the bremsstrahlung end-point energies of 8-17.3 MeV was calculated from the observed photo-peak activity (A_{obs}) using Eq. (4). The DPS was converted to activity in micro Curie (μCi) per gram of ^{nat}U and ^{nat}Mo for 24 hours of irradiation and are given in Table 3.

Theoretical calculation of ^{99}Mo activity using the photo-fission (reaction) cross-section, fission yield and estimated photon flux.

In order to examine the feasibility of commercial scale, the activity for ^{99}Mo production in the ^{nat}U(γ, f) and ^{nat}Mo(γ, n) reactions per gram of the sample in 24 hours of irradiation for end-point bremsstrahlung energy of 10-25 MeV was calculated as follows

In the case of ^{nat}U(γ, f) reaction, the initial activity (A_i) of ^{99}Mo is given as

$$A_i = N\langle\sigma_F\rangle\Phi Y (1 - e^{-\lambda t}) \quad (5)$$

In the case of ^{nat}Mo(γ, n) reaction, the initial activity (A_i) of ^{99}Mo is given as

$$A_i = N\langle\sigma_R\rangle\Phi (1 - e^{-\lambda t}) \quad (6)$$

All the terms in Eqs. (5) and (6) have the same meaning as given in Eqs. (1) and (2).

It can be seen from Eqs. (5) and (6) that calculations of activity of ^{99}Mo at the bremsstrahlung end-point energies of 10-25 MeV needs information's such as ^{nat}U(γ, f) and ^{nat}Mo(γ, n) reactions cross-sections ($\langle\sigma_{F(R)}\rangle$), cumulative yields of ^{99}Mo and the photon flux during the irradiation. In the 10-25 MeV bremsstrahlung induced fission of ^{238}U, the cumulative yields of ^{99}Mo was taken from refs. [42-52]. The bremsstrahlung spectra as a function of photon energy from a 10-25 MeV electron beam was calculated using GEANT4 computer code [56]. The ^{238}U(γ, f) and ^{100}Mo(γ, n) reaction cross-sections as a function of photon energy was obtained from TALYS computer code version 1.6 [59].

TALYS [59] can be used for the calculation of nuclear reactions and fission cross-sections that involve (i) targets of 12 mass units and heavier and (ii) projectiles such as photons, neutrons, protons, ^{2}H, ^{3}H, ^{3}He and alpha particles in the energy range of 1 keV to 200 MeV. In TALYS, several options are included for the choice of fission barrier parameters. In the present work, we calculated the photon-induced fission cross-section (σ_F(E)) of ^{238}U target using the default option of the fission parameters in the TALYS code [59], ignoring the symmetric fission mode. The default parameters in the TALYS code define the asymmetric fission barrier. The inner and outer fission barrier values used in the present calculation for ^{238}U were 6.3 MeV and 5.5 MeV respectively. The

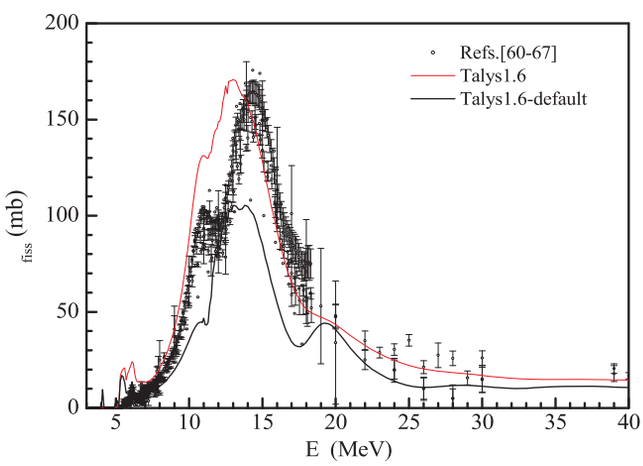

Fig. 5: Plot of ^{238}U(γ, f) reaction cross-section from TALYS 1.6 code and experimental data [60-67]

Table 3. Experimentally obtained ^{99}Mo activity in μCi in the ^{nat}U(γ, f) and ^{nat}Mo(γ, n) reactions per gram of the target for 24 hours irradiation in different electron LINAC.

Experimental work carried out at	End-point bremsstrahlung energy (MeV)	Activity of ^{99}Mo (μCi) from ^{nat}U(γ, f) reaction per g for 24 hours irradiation	Activity of ^{99}Mo (μCi) from ^{nat}Mo(γ, n) reaction per g for 24 hours irradiation
Microtron (Mangalore,India)	8.0	0.0255±0.0013	--
EBC (Kharghar, India)	10.0	0.309±0.050	0.318±0.048
SAPHIR (CEA, France)	11.5	0.369±0.013	--
ELBE (Dresden, Germany)	12.0	--	0.183±0.001
SAPHIR (CEA, France)	13.4	0.452±0.021	--
ELBE (Dresden, Germany)	14.0	--	0.823±0.073
SAPHIR (CEA, France)	15.0	0.545±0.027	--
ELBE (Dresden, Germany)	16.0	--	4.292±0.288
SAPHIR (CEA, France)	17.3	0.735±0.011	--

transmission coefficients through fission barriers were calculated with the Hill-Wheeler formula. All possible outgoing channels for a given γ-ray energy were considered. However, the cross-section for the photo-fission was carefully examined. The partial-wave cross-sections for the $J^{\pi}K=1^{-}0$, $1^{-}1$ and $2^{+}0$ photo-fission channels were included to determine the total photo-fission cross-section. The photon-induced fission cross-sections of ^{238}U obtained from the TALYS calculations are plotted in Fig. 5 along with the experimental data from refs. [60-67]. The ^{100}Mo(γ, n) reaction cross-section was also calculated using TALYS code [57] using default parameters. The ^{100}Mo(γ, n) reaction cross-section as a function of photon energy is given in Fig.6 along with the experimental data from Ref. [38].

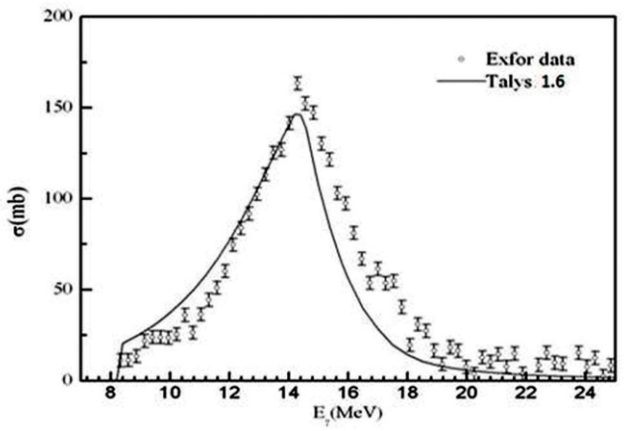

Fig. 6. Plot of ^{100}Mo(γ, n) reaction cross-section from TALYS 1.6 code and experimental data [38]

It can be seen from Figs. 5 and 6 that the ^{238}U(γ, f) and ^{100}Mo(γ, n) reactions cross-sections calculated using TALYS model show a structure similar to the experimental value [60-67, 38]. In the case of ^{100}Mo(γ, n) reaction, the cross-section from TALYS calculation are comparable to experimental value [38] with slight shift towards the lower energy side. However, in the case of ^{238}U(γ, f) reaction, the magnitude of fission cross-section from TALYS calculation are lower compared to the experimental value [60-67]. This is probably due the default parameters such as inner fission barrier of 6.3 MeV and outer fission barrier of 5.5 MeV used in the TALYS calculation. However, in the case of ^{238}U(γ, f) reaction, both the inner and outer fission barriers have been taken as 5.7 MeV [68]. In view of that the fission cross-section for the ^{238}U(γ, f) reaction was also calculated using level density model-2, shell model-2 and both fission barrier of 5.7 MeV [68] and plotted in Fig. 5. The values from TALYS are now comparable with the experimental data [61-68] but with slight shift towards the lower energy side. Thus the flux weighted average fission ($<\sigma_F>$) and reaction ($<\sigma_R>$) cross-sections for the ^{238}U(γ, f) and ^{100}Mo(γ, n) reactions were calculated from the both experimental [60-67, 38] and theoretical cross-section using the following equation.

$$<\sigma_F> = \Sigma(\sigma_F\,\Phi)/\Sigma\Phi \quad \text{and} \quad <\sigma_R> = \Sigma(\sigma_R\,\Phi)/\Sigma\Phi \qquad (7)$$

Further, it can be also seen from the Figs. 5 and 6 that the threshold value for the ^{238}U(γ, f) and ^{100}Mo(γ, n) reactions are 4 MeV and 8.29 MeV respectively. Thus the flux weighted average fission cross-section ($<\sigma_F>$) for ^{238}U(γ, f) reaction was calculated above threshold value of 4 MeV. In the case of ^{100}Mo(γ, n) reaction, the flux weighted average reaction cross-section ($<\sigma_R>$) was calculated above the threshold value of 8.29 MeV. At the bremsstrahlung end-point energy of 10 MeV, the flux weighted average fission cross-section for the ^{238}U(γ, f) reaction are 6.75 mb and 13.87 mb using the experimental [60-67] and TALYS cross-section data above threshold value of 4 MeV. In the case of ^{100}Mo(γ, n) reaction, the flux weighted average reaction cross-sections are obtained as 0.17 barns and 0.025 barns using the experimental [38] and TALYS cross-section data above threshold value of 8.29 MeV.

The photon flux used in the calculation was 1.0×10^{13} photon $cm^{-2}\ s^{-1}$. This is based on the conversion coefficient of 40% for an average electron beam current of one mA with a frequency of 400 Hz and a pulse width of 10 μs. For 1mA current, the power rating of the machine depends on the energy of the beam, which is 100 watts for 25 MeV beam energy of 1 mA current. For other beam energies, the beam power can be obtained proportionally ((E/25)x100 watts). The bremsstrahlung end-point energies of 10-25 MeV was chosen because the cross-section for the ^{nat}U(γ, f) and ^{nat}Mo(γ, n) reactions are significant within 10-20 MeV and have a maxima around 13-15 MeV due to GDR cross-section. The bremsstrahlung spectra as a function of photon energy from a 10-25 MeV electron beam were calculated using GEANT4 computer code [56] as mentioned before. Since the threshold energy for the ^{nat}U(γ, f) and ^{nat}Mo(γ, n) reactions are 4 MeV and 8.29 MeV, the photon flux ratio above these energies to total flux was used, which is shown in the fourth column of the Table 4. The flux weighted average fission ($<\sigma_F>$) and reaction ($<\sigma_R>$) cross-sections for ^{238}U(γ, f) and ^{100}Mo(γ, n) reactions were obtained by using the experimental cross-section for

Table 4: Comparison of ^{99}Mo activity calculated from ^{nat}U(γ, f), ^{nat}Mo(γ, n), ^{nat}U($n_{1.9\ MeV}$, f), ^{nat}Mo(n_{th}, γ) and ^{235}U(n_{th}, f) reactions for 24 hours irradiation of one gram sample with total flux (Φ) of 1.0×10^{13} photon (neutron) $cm^{-2}\ s^{-1}$. The photon flux is produced from the focused electron beam without scanning the position of the electron beam in the exit window of the accelerator.

Reaction Type	Incident Energy	Cumulative Yields of ^{99}Mo In % [Ref.]	Ratio of Φ >4(8.29) MeV To total	<σ> in mb Expt (TALYS)	Activity of ^{99}Mo (μCi)
^{nat}U(γ, f)	10 MeV	5.72 [42,52]	0.09949	6.75 (13.87)	5.8 (11.9)
	11 MeV	6.76 [46]	0.11354	10.79 (19.03)	12.5 (22.1)
	15 MeV	6.13 [46]	0.15681	26.98 (42.47)	39.3 (61.9)
	20 MeV	6.17 [46]	0.19663	40.48 (50.86)	74.4 (93.5)
	25 MeV	6.48 [47]	0.22473	41.75 (51.08)	85.0 (104.0)
^{nat}U(n, f)	1.9 MeV	6.28 [3]	0.01	500	47.9
^{nat}Mo(γ, n)	10 MeV	--	(0.0117)	17.03 (25.67)	7.2 (10.9)
	11 MeV	--	(0.0206)	20.51 (30.88)	15.3 (23.1)
	15 MeV	--	(0.0535)	51.06 (58.53)	99.2 (115.7)
	20 MeV	--	(0.0876)	59.11 (59.74)	188.1 (190.1)
	25 MeV	--	(0.1192)	50.52 (55.27)	218.7 (239.3)
^{nat}Mo(n, γ)	0.025 eV	--	--	130	12000
^{235}U(n, f)	0.025 eV	6.18 [71]	--	584000	5.57 x10^6

mono-energetic photon from Refs. [60-67, 38] and are shown in the fifth column of the Table 4. The $<\sigma_F>$ for the $^{238}U(\gamma, f)$ reaction and $<\sigma_R>$ for the $^{100}Mo(\gamma, n)$ reaction obtained from TALYS calculation are given in sixth column. The cumulative yields of ^{99}Mo (4.835-6.48%) in the 10-25 MeV bremsstrahlung induced fission of ^{238}U was taken from Refs. [42-52]. The calculated activity (A_i) of ^{99}Mo in the $^{nat}U(\gamma, f)$ and $^{nat}Mo(\gamma, n)$ reactions for 24 hours of irradiation time per one gram of natural sample and end-point bremsstrahlung energies of 10-25 MeV is given in the last two columns of the Table 4 using the $<\sigma_F>$ and $<\sigma_R>$ values from the experiment and TALYS of the fifth columns.

Calculation of elution yields from the radiochemical separated samples

The activity of ^{99}Mo and ^{99m}Tc in the undissolved samples and ^{99m}Tc in the separated samples were estimated by off-line γ-ray spectrometric technique using pre-calibrated HPGe detector coupled to a PC based 4K-channel analyzer in live time mode. The elution yields from the irradiated molybdenum oxide and zirconium molybdate gel are given in Table 5 and 6, respectively.

Table 5: The ^{99m}Tc yield from the irradiated Molybdenum trioxide by solvent extraction process

Generator	Elution No.	Time after EOB (hours)	^{99m}Tc activity in unseparated target solution (kBq)	Eluted ^{99m}Tc (kBq)	Elution Yield (%)
Irradiation 1 - 10MeV					
MoO_3 ; 0.23 grams; MEK phase	1	24	0.028	0.0198	70.7
Irradiation 2 – 15 MeV					
MoO_3 ; 0.53 grams; MEK phase	1	46	7.9	5.61	71
Irradiation 3 – 15 MeV					
MoO_3 ; 0.6 grams; MEK phase	1	45	5.8	4.2	72.4
Irradiation 4 – 15 MeV					
MoO_3; 0.5 grams; MEK phase	1	52	12.1	9.1	75.2

Table 6: The ^{99m}Tc elution yield from the irradiated Zirconium molybdate gel

Generator	Elution No.	Time between elutions / EOB (hours)	^{99m}Tc activity in unseparated target (kBq)	Eluted ^{99m}Tc (kBq)	Elution Yield (%)
Irradiation 1 – 10 MeV					
Zirconium molybdate; 1 gram; eluent saline	1	47	0.0469	0.00896	19.1
Irradiation 2 – 15 MeV					
Zirconium molybdate; 6 grams; eluent saline	1	45	45.1	15.17	33.6
	2	21	33.4	10.36	31
	3	55	25.6	6.12	23.8
	4	19.5	14.4	4.14	28.75
	5	25	11.7	3.075	26.3
Irradiation 3 – 15 MeV					
Zirconium molybdate; 3 grams; eluent acetone	1	44	14.53	4.3	29.6
	2	24	10.4	3.65	35
	3	11	6.5	2.28	35.1
Zirconium molybdate; 3 grams; eluent saline	1	42	14.5	3.85	26.55
	2	24	10.5	3.81	36.2
	3	11	6.6	1.857	28.1
Irradiation 4 – 15 MeV					
Zirconium molybdate; 3 grams; eluent saline	1	50	36.89	12.2	32.99
	2	36	23.9	7.1	29.7
	3	31	17.4	4.27	24.5
	4	41	10.2	2.93	28.7
	5	72	4.8	1.58	33
	6	96	1.4	0.61	43

Discussion

It can be also seen from the Table 4 that the calculated activity of ^{99}Mo for 24 hours of irradiation per gram of sample in the ^{nat}U(γ, f) reaction is lower than that in the ^{nat}Mo(γ, n) reaction, very much similar to the values shown in Table 3. Further, it can be seen from Table 4 that for the bremsstrahlung end-point energy of 20 MeV, the calculated activity of ^{99}Mo is about 190 μCi from ^{nat}Mo(γ, n) reaction, which is comparable with the value of 236 μCi of Ref. [35]. It can be also seen from Table 4 that for the bremsstrahlung end-point energy of 10 MeV, the activity of ^{99}Mo in the ^{238}U(γ, f) and ^{nat}Mo(γ, n) reactions are about 20 times higher than the experimental value shown in Table 3. This is because of the difference of photon flux of 20 times between Table 3 and Table 4. This arises due to 5 cm wide scanning electron beam of oscillation frequency 10 times per second over 50 cm length. In one sweep, the electron beam covers an area of 2x5x50 =500 cm^2 covering the forward and backward oscillation. Therefore the fraction of beam on sample of one cm^2 =2x1 cm^2/500 cm^2 =1/25. Thus with the focused beam, the activity of ^{99}Mo produced is higher by a factor of 25 times in the case of ^{nat}U(γ, f) and ^{nat}Mo(γ, n) reactions of the estimated value (Table 4) compared to the experimental value (Table 3).

In table 4, the activities of ^{99}Mo produced in the ^{nat}U(γ, f) and ^{nat}Mo(γ, n) reactions are also compared with the data in the ^{nat}U(n, f) and ^{98}Mo(n, γ) reactions. For this purpose, the activity of ^{99}Mo in the ^{nat}U(n, f) reaction was calculated using Eq. (5) at a neutron energy of 1.9 MeV, which is the average energy of epi-cadmium neutron spectrum [69, 70]. The ^{238}U(n, f) reaction cross-section used at this neutron energy was 0.5 barns [3] with a total neutron flux of 1.0x10^{13} n cm^{-2} s^{-1}. Since ^{238}U undergoes fission with only fast neutrons, the ratio of epi-cadmium to total neutron flux of 0.01 [70] was used. Similarly, the activity of ^{99}Mo in the ^{98}Mo(n, γ) and ^{235}U(n, f) reactions was calculated using a thermal neutron flux of 1.0x10^{13} n cm^{-2} s^{-1}. For the thermal neutron energy, the cross-section of 0.13 barns for the ^{98}Mo(n, γ) reaction and 584 barns for the ^{235}U(n, f) reaction used in the calculation were taken from Ref. [3]. The cumulative yield of ^{99}Mo for the ^{238}U(n, f) reaction was taken from Refs. [42-52], whereas for the ^{235}U(n_{th}, f) reaction, it was taken from Ref. [71]. The activity of ^{99}Mo produced per 24 hours of irradiation time per gram of the sample with total flux of 1.0x10^{13} neutrons or photons cm^{-2} s^{-1} from different reactions are given in Table 4.

From Table 4, it can be seen that the activity of ^{99}Mo in the ^{235}U(n_{th}, f) reaction is much larger than any other reaction. In conventional way, activity of ^{99}Mo is usually produced in thermal neutron induced fission of ^{235}U but not in the fast neutron induced fission of ^{238}U. This is because the fission cross-section of ^{238}U(n, f) with fast neutron induced is only 0.5-2 b [3], whereas for the ^{235}U(n, f) reaction with thermal neutrons is significantly high (584 b) [3]. Besides this, the thermal neutron production with high flux is well established in conventional research reactor [14]. Thus the thermal neutron induced fission of ^{235}U is a very good route for ^{99}Mo production, which fulfils the present demand of the world. However, high enriched ^{235}U (HEU) of 93 % is primarily weapons-grade, very expensive and have restriction by IAEA for ^{99}Mo production. The HEU is also alpha active and is thus hazardous from a safety and proliferation point of view. In order to avoid weapon grade ^{235}U, the activity of ^{99}Mo can be produced from the low enriched uranium (LEU) of 20-46% [14]. However, production of ^{99}Mo in the ^{235}U(n_{th}, f) reaction using HEU or LEU is not favourable with respect to the cost, safety, licensing and complications to make a reactor. From LEU target, production of ^{99}Mo in the ^{235}Un$_{th}$, f) reaction is associated with some ^{239}Pu contamination due to the ^{238}U(n, γ) reaction followed by two successive beta decay. The ^{239}Pu production and contamination is hazardous for medical application. Production of ^{99}Mo in the fast neutron induced fission of ^{238}U is also associated with some ^{239}Pu in the ^{238}U(n, γ) reaction followed by two successive beta decay. Besides this, generating a higher neutron flux for fast neutron induced fission of ^{238}U is possible only in the fast reactors or Accelerated Driven Sub-critical system (ADSs), which is an expensive, difficult option and not yet established. Thus production of ^{99}Mo activity in the fast neutron induced fission of ^{238}U is so far not done. Further, it can be seen from Table 4 that the activity of ^{99}Mo in the ^{nat}U(n, f) reaction is lower compared to the ^{nat}U(γ, f) reaction. The production of ^{99}Mo activity in the ^{nat}U(γ, f) reaction can be increased by obtaining a higher photon flux from an electron LINAC, which can be achieved by increasing the electron beam current. Thus producing ^{99}Mo activity in the ^{nat}U(γ, f) reaction is a potential alternative compared to the ^{235}U(n, f) reaction from a safety point of view, in spite of the lower activity in the former than later. However, in the case of the ^{nat}U(γ, f) reaction also radioactive waste of 50 Ci is generated per one Ci of ^{99}Mo activity production. Thus production of ^{99}Mo activity in the ^{nat}Mo(γ, n) reaction is the better option from the point of low radioactive waste generation.

It can be also seen from Table 4 that production of ^{99}Mo activity in the ^{nat}Mo(γ, n) reaction is more attractive than the ^{nat}Mo(n, γ) route in spite of its lower specific activity. The cross-section of ^{100}Mo(γ, n) reaction is 0.128-0.1523 barns for the photon energy of 13.-15 MeV [38], which is comparable to the value of 130 mb for the ^{98}Mo(n, γ) reaction for thermal neutron [3]. The lower specific activity of ^{99}Mo in the ^{nat}Mo(γ, n) reaction is due to the higher reaction threshold of 8.29 MeV for the ^{100}Mo(γ, n) reaction and lower bremsstrahlung flux-weighted average reaction cross-section. Besides this, the isotopic abundance of ^{100}Mo in ^{nat}Mo is only 9.6% compared to the value of 24.4% for ^{98}Mo. The lower activity of ^{99}Mo in the ^{100}Mo(γ, n) reaction route in ^{nat}Mo can be compensated by increasing the photon flux with an increase of electron current or by using enriched ^{100}Mo. An accelerator (electron LINAC) facility for ^{99}Mo production will require substantially more

electric power to run than a reactor-based facility. The multi-kilowatt electron accelerator with focused beam has a problem of heating effect, which will lead to an issue of cooling arrangement. This can be solved by scanning the electron beam with an appropriate cooling arrangement and using a number of small targets instead of a single large target. Further, the use of enriched ^{100}Mo enhance the production of ^{99}Mo ten times in the ^{100}Mo(γ, n) reaction compared to the ^{nat}Mo(γ, n) reaction. There are two facilities that can produce large quantities of ^{100}Mo using gas centrifuges [34]. The present cost of $2000 per gram for ^{100}Mo is much less than the cost of the electron accelerator. This cost will drop significantly on large scale production [34]. The enriched ^{100}Mo target in the world market is available from different vendors with the cost of $400-600 per gram when purchased in large quantity [72]. Besides this, the irradiated enriched ^{100}Mo sample can be reused after 40 days of irradiation time and after separating its daughter ^{99m}Tc at different time depending upon the need.

From chemical separation point of view, it can be seen from Table 5 and 6 that the chemical yield of the separated ^{99m}Tc from the dissolved molybdenum trioxide is 70.7-75.2%, whereas in the undissolved zirconium molybdate gel, it is 19.1-43%. In spite of the low chemical yield, the separation of ^{99m}Tc from the undissolved zirconium molybdate gel is preferable over the dissolved molybdenum trioxide because the separation is user friendly and the generator can be used in hospital radiopharmacy throughout the shelf-life. The production yield of ^{99m}Tc is from the present work is around kBq/mL or kBq/g target, whereas dose applicable for a single injection dose used in nuclear medicine imaging is ~300-1000 MBq. The scaling up of ^{99}Mo- ^{99m}Tc activity to clinical levels would be achievable with increase of target material, enrichment, beam power, irradiation time and scanning electron beam.

The production of ^{99}Mo in the ^{nat}U(γ, f), ^{nat}Mo(γ, n) and ^{100}Mo(γ, n) reactions has many advantages compared to the existing method of commercial production. With the above mentioned solutions, production of ^{99}Mo in the ^{100}Mo(γ, n) reaction from enriched molybdenum is an attractive alternative to the ^{235}U(n_{th}, f) reaction. In the absence of enriched ^{235}U and ^{100}Mo isotopes, production of ^{99}Mo in the ^{nat}U(γ, f) and ^{nat}Mo(γ, n) reactions is very much useful and can fulfil the increasing demand of this important isotope. In particular, it is possible to install electron LINAC at a lower cost, very near to the medical centres, which reduces the transport time and does not need enhanced security and other safe guards unlike nuclear reactors. Besides this, it is possible to halt and re-start the accelerator for isotope production through the ^{nat}U(γ, f) and ^{nat}Mo(γ, n) reaction routes as per the demand, something that cannot be achieved with a nuclear reactor through the ^{235,238}U(n, f) and ^{98}Mo(n, γ) reaction routes.

From Table 3, it can be seen that the activity of ^{99}Mo per day per gram is around 0.32 μCi using 4 kW electron LINAC at EBC, Kharghar, with 400 Hz repetition rate with 10 μs pulse width and only area of 1 cm^2 sample size. Scanning beam is 10 Hz, covering twice an area of 500 squares cm per one oscillation (back and forth). Based on DOE estimate, the world demand ^{99}Mo activity is about 500 Ci per day [73]. It can be seen from Table 4, that the activity of ^{99}Mo in the ^{nat}Mo(γ, n) reaction, with electron linac of 4 kW power and a beam current of 60 mA, is comparable to that of the ^{98}Mo(n, γ) reaction route. Thus to fulfil the demand of DOE, it would be necessary to have 100 electron linac of 10 kW beam power irradiating the enriched ^{100}Mo targets of 10 grams each. This high beam power of 10 kW for electron linac having a scanning beam is distributed over 500 cm^2 area of the target. This will solve the heat dissipation problem of focused beam, which otherwise cannot be handle by present technology. This can be solved by scanning the electron beam with an appropriate cooling arrangement and using a number of small targets over an area of 500 cm^2 instead of a single large target. Further, the activity of ^{99}Mo could be increased by taking sandwiched targets of pure ^{100}Mo and ^{nat}U, which could reduce the number of electron linac required.

Conclusions

(I) The medical isotope ^{99}Mo which has a half-life of 65.94 hours was experimentally produced in the ^{nat}U(γ, f) reaction for the bremsstrahlung end-point energies of 8-17.3 MeV and in the ^{nat}Mo(γ, n) reaction for 8-70 MeV. The experimentally produced activity of ^{99}Mo in the ^{nat}U(γ, f) reaction was found to be slightly lower than in the ^{nat}Mo(γ, n) reaction.

(ii) A radiochemical separation procedure of ^{99m}Tc from its generator ^{99}Mo in the irradiated natural molybdenum trioxide (MoO_3) and zirconium molybdate gel was also developed. The chemical yield of the separated ^{99m}Tc from the dissolved molybdenum trioxide is 70.7-75.2%, whereas in the undissolved zirconium molybdate gel, it is 19.1-43%. In spite of the low chemical yield, the separation of ^{99m}Tc from the second method is preferable because the separation is user friendly and the generator can be used in hospital radiopharmacy throughout the shelf-life.

(iii) The activity of ^{99}Mo produced in the ^{nat}U(γ, f) and ^{nat}Mo(γ, n) reactions are calculated by using the estimated photon flux and TALYS flux-weighted cross-sections for the ^{nat}U(γ, f) and ^{nat}Mo(γ, n) reactions respectively. It was found that the ^{99}Mo produced in the ^{nat}U(γ, f) and ^{nat}Mo(γ, n) reactions with the bremsstrahlung obtained from scanning electron beam is better than the focused electron beam from the point of view of cooling the target and thus is important for its practical application.

(iv) The photo-neutron (^{nat}Mo(γ, n)) and photo-fission (^{nat}U(γ, f)) reactions channels provide an alternative route to the ^{98}Mo(n, γ) and ^{235,238}U(n, f) reactions channels circumventing the need for a reactor. Thus it is possible to fulfil the DOE medical requirements of ^{99}Mo by the photo-reaction of ^{nat}Mo or ^{100}Mo and photo-fission of ^{nat}U.

Acknowledgement

The authors are thankful to the staff of the microtron at Mangalore, Karnataka India, electron linacs at EBC, Kharghar Navi-Mumbai, India, ELBE at HZDR, Dresden, Germany, SAPHIR at CEA, Saclay, France and PAL, Pohang, South Korea for providing the electron beam to carry out the experiments. We are thankful to the IAEA for giving the IAEA-CRP project No. 17443/R0 and BRAIN pool program under KOFEST, Korea, for inviting him as visiting professor to the department of high-energy physics, Daegu, as well as giving financial support to travel to Dresden, Germany, to carry out the experiment.

References

1. O. Hahn and F. Strassmann, Naturwiss **27**, 11 (1939)
2. R. O. Haxby, W. E. Shoupp, W. E. Stephens, and W. H. Wells, Phys. Rev. **59**, 57 (1941)
3. S.F. Mughabghab, M. Divadeenam, N.E. Holden, *Neutron resonance and thermal cross sections*, Vol. **I** (Academic Press, New York, 1981).
4. IAEA, *Handbook on photonuclear data for applications cross-sections and spectra*, IAEA TECDOC-1178 (IAEA, Vienna, 2000) available online at http://www-nds.iaea.org/publications/tecdocs/.
5. IAEA, *Nuclear technology review, annex VIII: The socioeconomics of nuclear applications: a perspective* (IAEA, Vienna, 2004) pp. 85–94.
6. IAEA, *Categorization of radioactive sources* - Revision of IAEA-TECDOC-1191 and IAEA-TECDOC-1344 (IAEA, Vienna, 2003).
7. National Council of Radiation Protection and Measurements (NCRP), *Sources and magnitude of occupational and public exposures from nuclear medicine procedures*, NCRP report no. 124, March 1996.
8. S. Groth, *Lasting benefits: Nuclear application in health care*, IAEA Bulletin, 42/1/2000, Vienna (2000).
9. C.L. Larsson *Availability and Use of Medical Isotopes in Canada*, TM 2004-218, OMB no. 0704-0188 (Defense Research and Development Canada (DRDC), Ottawa, 2004).
10. C. Schiepers, *Diagnostic Nuclear Medicine* (Springer, Berlin, 2006).
11. IAEA, *Alternative technologies for 99mTc generators*, IAEA-TECDOC-852 (IAEA, Vienna, 1995) http://wwwpub. iaea.org/MTCD/publications/PDF/te852 prn.pdf.
12. IAEA, *Charged particle cross-section data base for medical radioisotope production: diagnostic radioisotopes and monitor reactions*, IAEA-TECDOC-1211 (IAEA, Vienna, 2001) http://www-nds.iaea.org (accessed May 2001).
13. T. Ruth, Accelerator production of medical isotopes, Nature **457**, 536 (2009).
14. IAEA, *Nuclear technology review, annex VIII: Production and supply of molybdenum-99*, IAEA/NTR/2010 (IAEA, Vienna, 2010) pp. 150–167.
15. J.P. Gambini, P. Cabral, O. Alonso, E. Savio, S.D. Figueroa, X. Zhang, M. Lixin, L.D. Susan, P.Q. Thomas, Nucl. Med. Biol. **38**, 255 (2011).
16. M.A. Ter´an, M. Elena, A.L Reyes, P. Andrea, V. Marcelo, E. Patricia, P.P. Jose, S. Eduardo, Nucl. Med. Biol. **38**, 279 (2011).
17. NuDat 2.6, National Nuclear Data Center, Brookhaven National Laboratory, updated 2011, available on-line at http://www.nndc.bnl.gov/.
18. R.B. Firestone, L.P. Ekstrom, *Table of Radioactive Isotopes*, Lawrence Berkeley National Laboratory, Berkeley Version 2.1 (2004) http://ie.lbl.gov/toi/index.asp.
19. W.Z. Villiers, The management of radioactive waste from fission Mo-99 production. Int.Top Meet. Nucl. Hazard Waste Manag. 2190–2192 (1994).
20. J. Bourges, C. Madic, G. Koehly, H. Nguyent, D. Baltes, C. Landesman, A. Simon, Nucl. Technol. **113**, 204 (1996).
21. M.M. Rahman, S.M. Qaim, Nucl. Phys. A **435**, 43 (1985).
22. P. Reimer, V. Avrigeanu, S.V. Chuvaev, A.A. Filatenkov, T. Glodariu, A. Koning, A.J.M. Plompen, S.M. Qaim, D.L. Smith, H. Weigmann, Phys. Rev. C **71**, 044617 (2005).
23. M.C. Lagunas-Solar, P.M. Kiefer, O.F. Carvacho, C.A. Lagunas, Y.P. Cha, Cyclotron production of NCA 99mTc and 99Mo. An alternative non-reactor supply source of instant 99mTc and 99Mo→ 99mTc generators, Appl. Radiat. Isot. **42**, 643 (1991).
24. M.C. Lagunas-Solar, N.X. Zeng, I. Mirshad, T. Grey-Morgan, Cyclotron production of molibdenum-99 via proton-induced uranium-238 fission. J. Am. Nucl. Soc. **74**, 134-335 (1996).
25. M.C. Lagunas-Solar, *Accelerator production of* 99*mTc with proton beams and enriched* 100*Mo targets*, IAEA TECDOC, Vol. **1065** (IAEA, Vienna, 1999) p. 87.
26. B. Scholten, R.M. Lambrecht, C. Michel, V.R. Hernan, S.M. Qaim, Excitation functions for the cyclotron production of ^{99m}Tc and ^{99}Mo, Appl. Radiat. Isot. **51**, 69 (1999).

27. S. Tak´acs, Z. Szucs, F. T´ark´anyi, A. Hermanne, M. Sonck, Evaluation of proton induced reactions on 100Mo: New cross sections for production of 99mTc and 99Mo, J. Radioanal. Nucl. Chem. **257**, 195 (2003).

28. M.S. Uddin, M. Baba, Proton-induced activation cross-sections of the short-lived radionuclides formation on molybdenum, Appl. Radiat. Isot. **66**, 208 (2008).

29. Medical Isotope Production without Enriched Uranium (2009) Alternative molybdenum-99 production process; URL: http://www.nap.edu/openbook.phn

30. O. Lebeda, M. Pruszynski, New measurement of excitation functions for (p,x) reactions on natMo with special regard to the formation of 95mTc, 96m+gTc, 99mTc and 99Mo, Appl. Radiat. Isot. **68**, 2355 (2010).

31. R.G. Bennett et al., A system of 99mTc production based on distributed electron accelerators and thermal separation. Nucl. Technol. **126**, 102–121 (1999).

32. A.V. Sabel'nikov, O.D. Maslov, L.G. Molokanova, M.V. Gustova, S.N. Dmitriev, Preparation of 99Mo and 99mTc by 100Mo(γ,n) photonuclear reaction on an electron accelerator, MT-25 microtron, Radiokhimiya **48**, 172 (2006) or Radiochemistry **48**, 191 (2006).

33. A.V. Sabel'nikov et al., Preparation of 99Mo by 100Mo(γ, n) photonuclear reaction on an electron accelerator, MT-25 microtron. Radiochemistry 48:91. ISSN: 1066-3632 (2006).

34. C. Ross C et al., Using the ^{100}Mo photo-neutron reaction to meet Canada's requirement for 99mTc. La Phys Au Can 66(1) (2010).

35. D. Segey et al., Argonne activities for the production of Mo-99 using linac irradiation of Mo-100. In: RERTR 2010-32nd international meeting on reduced enrichment for research and test reactor, SANA Lisboa Hotel, Lisborn, Portugal, October 10–14 (2010).

36. D. Habs, U. K¨oster, Appl. Phys. B **103**, 501 (2011).

37. H. Utsunomiya, S. Goriely, T. Kondo, C. Iwamoto, H. Akimune, T. Yamagata, H. Toyokawa, H. Harada, F. Kitatani, Y.W. Lui, A.C. Larsen, M. Guttormsen, P.E. Koehler, S. Hilaire, S. Peru, M. Martini, A.J. Koning, Phys. Rev. C **88**, 015805 (2013).

38. H. Beil, R. Bergere, P. Carlos, A. Lepretre, A. De Miniac, A. Veyssiere, Nucl. Phys. A **227**, 427 (1974).

39. Rita Crasta, H. Naik, S.V. Suryanarayana, P.M. Prajapati, K.C. Jagadisan, S.V. Thakare, S. Ganesh, V.T. Nimje, K.C. Mittal, A. Goswami, J. Radioanal. Nucl. Chem. **290**, 367 (2011).

40. H. Naik, G.N. Kim, R. Schwengner, K. Kim, M. Zaman, S.C. Yang, S.G. Shin, Y.-U. Kye, R. Massarczyk, R. John, A. Junghans, A. Wagner, A. Goswami, M.-H. Cho, Eur. Phys. J. A **52**, 47 (2016).

41. H. Naik, G.N. Kim, R. Kapote Noy, R. Schwengner, K. Kim, M. Zaman, S.G. Shin, Y. Gey, R. Massarczyk,R. John, A. Junghans, A. Wagner, and M.-H. Cho, Eur. Phys. J. A **52**, 195 (2016).

42. H. Naik, V.T. Nimje, D. Raj, S.V. Suryanarayana, A. Goswami, S. Singh, S.N. Acharya, K.C. Mttal, S. Ganesan, P. Chandrachoodan, V.K. Manchanda, V. Venugopal, S. Banarjee, Nucl. Phys. A 853, 1 (2011).

43. H. Naik, Fr´ed´erick Carrel, G.N. Kim, Fr´ed´eric Laine, Adrien Sari, S. Normand, and A. Goswami, Eur. Phys. J. A **49**, 94 (2013).

44. H. Naik, B.S. Shivashankar, H.G. Raj Prakash, Devesh Raj, Ganesh Sanjeev, N. Karunakara, H.M. Somashekarappa, S. Ganesan and A. Goswami. J. Radioanal. Nucl. Chem. **299**, 127 (2014).

45. S. Pomme, E. Jacobs, K. Persyn, D. De Frenne, K. Govaert, M.L. Yoneama, Nucl. Phys. A 560, 689 (1993).

46. E. Jacobs, H. Thierens, A. De Frenne, A. De Clercq, P. D'Hondt, P. De Gelder, A.J. Deruytter, Phys. Rev. C 19, 422 (1979).

47. H. Thierens, D. De Frenne, E. Jacobs, A. De Clercq, P. D'Hondt, A.J. Deruytter, Phys. Rev. C 14, 1058 (1976).

48. D. Swindle, R. Wright, K. Takahashi, W.H. Rivera, L. Meason, Nucl. Sci. Eng. 52, 466 (1973).

49. A. Chattopadhyay, K.A. Dost, I. Krajbich, H.D. Sharma, J. Inorg. Nucl. Chem. 35, 2621 (1973).

50. L.H. Gevaert, R.E. Jervis, S.C. Subbarao, H.D. Sharma, Can. J. Chem. 48, 652 (1970).

51. H.G. Richter, C.D. Coryell, Phys. Rev. 95, 1550 (1954).

52. R.A. Schmitt, N. Sugarman, Phys. Rev. 95, 1260 (1954).

53. H. Naik, S.V. Suryanarayana, K.C. Jagadeesan, S.V. Thakare, P.V. Joshi, V.T. Nimje, K.C. Mittal, A. Goswami, V. Venugopal, S. Kailas, J. Radioanal. Nucl. Chem. **295**, 807 (2013).

54. A. Gopalakrishna, H. Naik, S. V. Suryanarayana, Y. Naik, V. T. Nimje, B. K. Nayak, S. K. Sarkar, S. Padmanabhan, C. Kothalkar, P. Naskar, A. C. Dey, A. Goswami, J Radioanal Nucl Chem 308, 431–438 (2016).

55. H. Naik, S.V. Suryanarayana and M.S. Murali, Photon, neutron and proton induced reactions to produce medical isotopes, IAEA-CRP-Project No. 17443/R0 (2012).

56. GEANT4 Collaboration (S. Agostinelli *et al.*), Nucl. Instrum. Methods A **506**, 250 (2003).

57. H.F. Royston, J.L. Jeremy, T. Pal Buckeley, L.D. Daniel, T.E. James, A. Paulenova, Radioisotopes in Medicine: Preparing a Technetium-99m Generator and Determining Its Efficiency, J. Chem. Educ. **83**, 625 (2006).

58. D.R. McAister and E.P. Horweitz, "Automated two column generator systems for medical radionuclide", App. Radiat. Isot., **67**, 1985 (2009).

59. A.J. Koning, S. Hilaire, M.C. Duijvestijn, *TALYS: comprehensive nuclear reaction modeling*, in: *Proceedings of the International Conference on Nuclear Data for Science and Technology-ND 2004*, edited by R.C. Haight, M.B. Chadwick, T. Kawano, P. Talou, Vol. **769** (AIP, New York, 2005) pp. 1154–1159.

60. A. Lepretre, R. Berger, P. Bourgeolis, P. Carlos, J. Fagot, J.L. Fallou, P. Garganne, A. Veyssiere, H. Ries, R. Gobel, U. Kneissl, G. Mank, H. Stroler, W. Wilk, D. Kyckbosch, J. Jury, Nucl. Phys. A **472**(1987) 533.

61. H. Ries, U. Kneissi, G. Mank, H. Stroher, W. Wilke, R. Berger, P. Bourgeois, P. Carlo, J.L. Fellou, P. Garganne, A. Veyssire, L.S. Cardman, Phys. Lett. B **139** (1984) 254.

62. H. Ries, G. Mank, J. Drexler, R. Hell, K. Huber,U. Kneissi, R. Ratzek, H. Stroher, J. Weber, W. Wilke, Phys. Rev. C **29** (1984) 2346.

63. J.T. Caldwell, E.J. Dowdy, B.L. Berman, R.A. Alvarez and P. Meyer, Giant resonance for the actinide nuclei: Photo-neutron and photo-fission cross sections for ^{235}U, ^{236}U, ^{238}U, and ^{232}Th, Phys. Rev. C **21** (1980) 1215.

64. P.A. Dicky, P.A. Akel, Phys. Rev. C **35** (1975) 501.

65. A. Veyssier, H. Bell, R. Berger, P. Carlos, A. Lepretre, Nucl. Phys. A **199** (1973) 45.

66. R.A. Anderl, J.E. Hall, R.C. Morrison, R.G. Struss, M.V. Yester, D.J. Zaffarano, Nucl. Phys. A **212** (1973) 221.

67. O.Y. Mafra, S. Kuniyoshi, J. Goldemberg, Nucl. Phys. A **186** (1972) 110.

68. S. Bjornholm and J.E. Lynn, The double-humped fission barrier, Rev. of Modern Phys. **52** (1980) 725.

69. H. Naik, A.G.C. Nair, P.C. Kalsi, A.K. Pandey, R.J. Singh, A. Ramaswami and R.H. Iyer, Absolute Fission Yields in the Fast Neutron Induced Fission of 99.9997 Atom % Pure ^{238}U Using Track Etch-Cum Gamma Spectrometric Technique, Radiochim. Acta. **75** (1996) 69.

70. R.H. Iyer, H. Naik, A.K. Pandey, P.C. Kalsi, R.J. Singh, A. Ramaswami, A.G. C. Nair, Measurement of Absolute Fission Yields in the Fast Neutron-Induced Fission of Actinides: ^{238}U, ^{237}Np, ^{238}Pu, ^{240}Pu, ^{243}Am and ^{244}Cm

71. T.R. England and B.F. Rider, "Evaluation and Compilation of Fission Products Yields," ENDF/BVI (1989).

72. S.D. Chemerisov, A.V. Galis, P.Tksec, D.L. Bowers, V. Makarashvili, A.J. Bakel, J.T. Harvey, G.E. Dale, G.F. Vandegrift, 32nd Interantional meeting on reduced enrichment for research and test reactor (rertr), October 10-14, 2010, SANA Lisboa Hotel, Lisbon, Portugal.

73. DOE solicitation titled "Molybdenum-99" DE-FOA-0000323, 04/29/2010.

Neutron Scattering Studies of Eco-friendly Functional Materials

S.K. Mishra, M.K. Gupta, R. Mittal, P.S.R. Krishna and S.L. Chaplot
Solid State Physics Division

Niobate based materials are environment friendly and appropriate for wide piezoelectric applications due to their piezo-response that is comparable to Pb(Zr Ti)O_3. Beyond the technological application, $NaNbO_3$ has been a rich model system for understanding of mechanisms of structural phase transitions when subject to changes in thermodynamical conditions like: temperature, pressure, and/or composition, particle size and external stimuli like electric/magnetic field etc. In the present work, we report systematic investigation of structural phase transitions with variations in temperature, external pressure and chemical pressure (via compositional modification) using the neutron scattering technique.

Keywords: structural phase transition, neutron scattering, ferro/antiferroelectric

Introduction

Materials exhibiting piezoelectric properties have been widely used in sensors and actuators. Most of the compounds used in these applications have lead as one of the constituents. Due to toxic nature of lead and environmental regulations, there is a need to replace lead. A considerable amount of research activity is directly aimed to explore lead –free piezoelectric materials. In this regards, alkaline niobate based solid solutions have shown considerable promise because they show ultrahigh piezo-response. Beyond the technological application, $NaNbO_3$ has been a rich model system for understanding of the mechanism of structural phase transitions. The present work combines state-of-the-art methodologies to understand the nature of phase transitions and identify the correlation between structure and phonon dynamics.

We have employed systematic neutron diffraction measurements as a function of temperature (T=12 K to 1050 K) and pressure to investigate the temperature/pressure induced structures and understand the sequence of structural phase transitions of $NaNbO_3$. Neutron diffraction offers certain unique advantages over x-ray diffraction especially in the accurate determination of positions of oxygen ions, which are crucial for resolving the controversies reported in the literature. The diffraction pattern of a polycrystalline sample shows a large numbers of peaks in intensity as a function of the angle of diffraction. Each peak may arise from one or more Bragg reflections from the crystallites. Any Bragg reflection is indexed by three integers (h,k,l), known as Miller indices, which tell us about the specific plane in the crystal which gives the Bragg reflection. After a phase transition new Bragg reflections may appear. In some cases, especially a second order phase transition, these new reflections may be due to change in the structure arising from freezing of some phonon vibrations.

The phonon modes that may condense or freeze are called soft phonons. A soft phonon is one whose frequency may tend to zero as we approach the phase transition. Softening of a phonon is also referred as phonon instability. Different phase transitions may be related to different soft phonons. The wave vector of the soft phonon is important in deciding the new frozen crystal structure. The wave vector may correspond to certain special points in the Fourier space (or reciprocal space). A primitive unit cell in the reciprocal space is called Brillouin Zone. As we discuss below, certain points like M (½ ½ 0), R (½ ½ ½), T (½, ½,¼) etc are of particular interest in case of $NaNbO_3$.

Based on our detailed temperature dependent neutron diffraction studies, the phase diagram of sodium niobate is presented that resolves existing ambiguities in the literature about the different structures. We have also shown for the first time direct experimental evidence of presence of antiferroelectric and ferroelectric instabilities at low temperature. We have investigated phase transitions induced by chemical substitution in $Li_x Na_{1-x} NbO_3$ system. We found that a variety of phases stabilized ranging from non-polar antiferrodistortive to ferroelectric and antiferroelectric in nature. The stability of various crystallographic phases could be understood in terms of phonon instabilities. In this context, the combination of inelastic neutron scattering and first-principles calculations forms an adequate framework to obtain accurately phonon frequencies. Both the experimental and computational techniques are helpful to understand the role of structural distortions and their correlation to phonon instabilities, leading to phase transitions in this material.

Temperature Induced Phase Transition

Neutron diffraction patterns of materials exhibiting perovskite structure contain two types of reflections: (1) the main perovskite reflections and the (2) super-lattice reflections due to the tilting of oxygen octahedra. Both types of reflections can be indexed with respect to a doubled perovskite unit cell. The super-lattice reflections assume Miller indices represented by one or more odd integers, while the main Bragg reflections are represented by all even

integered indices. Super-lattice reflections with all-odd integered indices, i.e., "ooo" type and two-odd and one-even integered indices (in Glazer's notation) result from anti-phase and in-phase tilting of the adjacent oxygen octahedra due to structural phase transitions driven by softening and freezing of the zone boundary phonons at R (q= ½, ½, ½) and M (q = ½, ½, 0) points of the cubic Brillouin zone, respectively

Figure 1 (a) depicts a portion of the powder neutron diffraction patterns of $NaNbO_3$ at some selected temperatures in the range from 12–975 K. At the highest temperature (T= 975 K), all the Bragg reflections present in powder diffraction patterns could be indexed as main cubic perovskite reflections. The reflection labeled as F in the diffraction pattern of cubic phase is from the furnace material. Below 950 and 900 K, two additional reflections called as "superlattice reflections" (S) marked with (S1) appear. Further, below 810 K, an additional set of superlattice reflections (S2) appear and some of them diminish followed by enhancement of the intensity of super lattice reflection (S3), which disappears below 680 K. Below 680 K, some of super lattice reflections vanish and new super lattice reflection (S4) appear. Superlattice reflections, in different temperature regime, are also present at higher angles with prominent intensities. The intensity of these super lattice reflections gradually decreases on lowering the temperature while some of the peaks show drastic changes in the diffraction data. Splitting in the peak around d= 2.25 Å (index as (111) in pseudo-cubic cell) appears into two peaks with the intensity ratio of 3:1, which is an unambiguous signature of rhombohedral distortions and reveals the stabilization of the ferroelectric (***R3c)*** phase at 25 K. Thus, disappearance and reappearance of superlattice reflections in the powder neutron diffraction provide unambiguous evidence for structural phase transitions in sodium niobate with temperature [4-5].

To examine the phase stability region, we have carried out detailed Rietveld analysis of temperature dependent powder neutron diffraction data. Our studies present unambiguous evidence for the presence of the ferroelectric ***R3c*** phase of $NaNbO_3$ coexisting with an antiferroelectric phase (***Pbcm)*** over a wide range of temperatures below 300 K (Fig. 1 (b &c). Theoretical lattice dynamics calculations of $NaNbO_3$ show that the potential energy barriers from the paraelectric ***Pm3m*** to antiferroelectric ***Pbcm*** and ferroelectric ***R3c*** phases are quite similar. New superlattice reflections appear at 680 K (R phase) and 770 K (S phase) [Fig. 1 (d)] that could be indexed using an intermediate long-period modulated orthorhombic structure whose lattice parameter along <001> direction is 3 and 6 times that of the $CaTiO_3$-like ***Pbnm*** structure respectively. The critical exponent (β) for the second order tetragonal to cubic phase transition about 950 K, corresponds to a value $\beta \approx {}^{1}/_{3}$, as obtained from the temperature variation of order parameters (tilt angle and intensity of superlattice

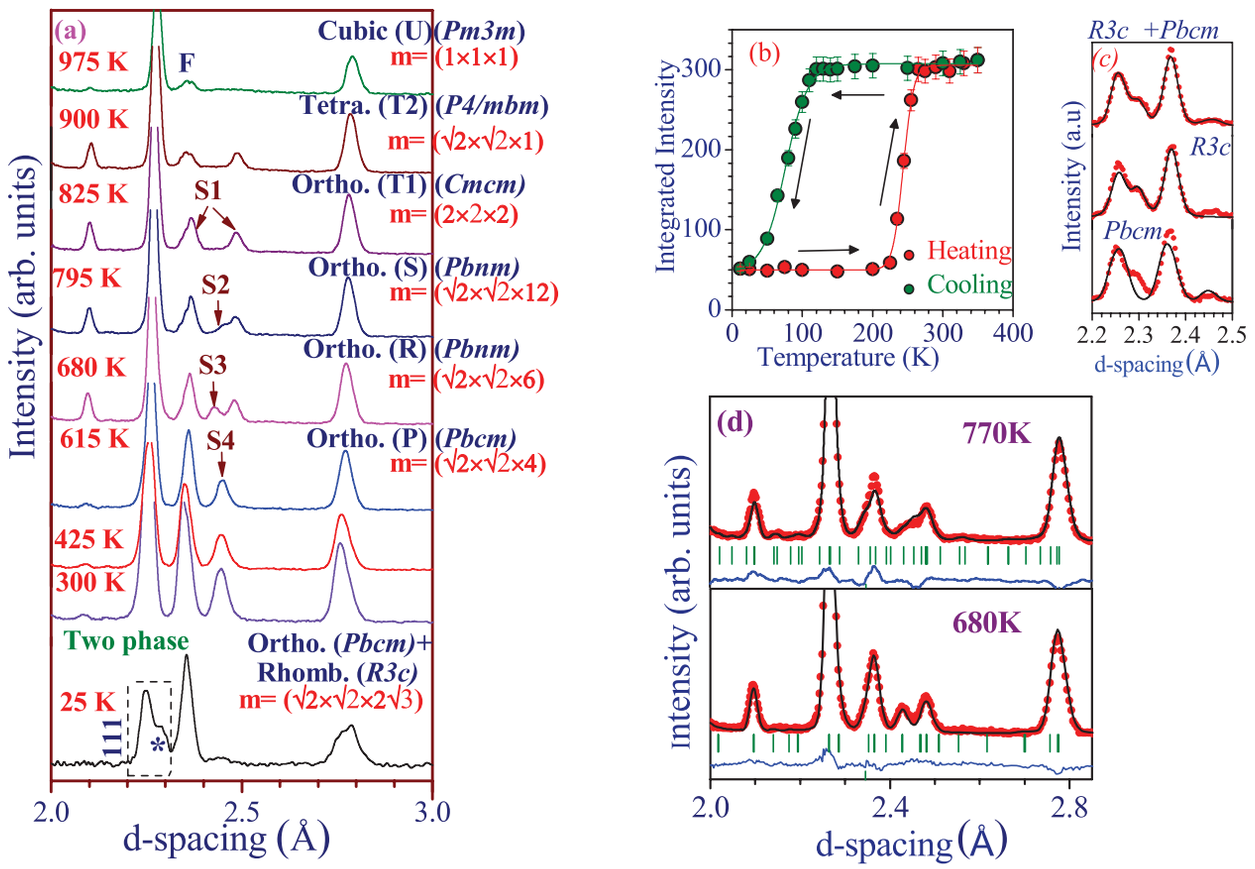

Fig. 1: (a) Evolution of neutron diffraction data [4,5] and phase stabilities region with temperature for $NaNbO_3$. Variation of integrated intensity of antiferroelectric peak (S4) is shown in (b). Observed (circle), calculated (continuous line), and difference (bottom line) profiles obtained after the Rietveld refinement of $NaNbO_3$ using (c) two phases (antiferroelectric orthorhombic Pbcm + ferroelectric rhombohedral R3c) at 12 K and (d) paraelectric orthorhombic Pbnm space group at 680 and 770 K.

reflections). It is argued that this exponent is due to a second order phase transition close to a tri-critical point. Based on our detailed temperature dependent neutron diffraction studies, the phase diagram of sodium niobate is presented that resolves existing ambiguities in the literature.

Pressure Induced Phase Transition

The hydrostatic pressure influence on ferroelectric (FE) and antiferrodistortive phase transitions has received considerable attention for materials exhibiting perovskite structure. The stability of the FE phase (driven by zone center instability at q=0) is reduced under pressure due to modification of the short-range interatomic and long range Coulomb interactions. On the other hand, the stability region of the antiferrodistortive phase (driven by the zone boundary instabilities at $q \neq 0$) expands with increasing pressure. Thus, it is interesting to investigate the effect of pressure on sodium niobate which has both competing (zone centre and boundary) instabilities simultaneously. Neutron diffraction patterns at room temperature were collected up to 11 GPa in pressure increasing cycle. To investigate the phase transitions, detailed Rietveld analysis of pressure dependent powder neutron diffraction data was carried out. $NaNbO_3$ has an antiferroelectric phase (***Pbcm***) at ambient condition. The paraelectric phase is found to stabilize above 8 GPa and its crystal structure has been determined in orthorhombic symmetry with space group ***Pbnm*** (Figure 2 left panel). Application of pressure changes the structural parameters such as the Nb–O bond length, Nb– O–Nb bond angles, and the distortion of the NbO_6 octahedra. Figure 2 (a) shows that the averaged Nb-O bond length shrinks almost continuously whereas a small jump of the Nb-O-Nb bond angle can be clearly seen at 8 GPa. It is evident from the figure that with increasing pressure, Nb-O2-Nb bond angle first increases upto 2GPa and then monotonically decreases upto 8 GPa. On the other-hand Nb-O1-Nb bond angle sharply decreases upto 2 GPa and then it decreases monotonically with increasing pressure (Fig. 2(b)). It is found that the tilt angle increases with increasing pressure with sharp enhancement above the phase transition pressure ($\approx$ 8 GPa). It could be noticed that the distortion in ***Pbnm*** phase is larger in comparison to that in Pbcm phase. We have not found evidence for a structural phase transition around 2 GPa as previously suggested in the literature based on Raman scattering experiments. However, significant changes in the Nb-O-Nb bond angles are found around this pressure. The response of the lattice parameters to pressure is strongly anisotropic with a largest contraction along <001>. The structural phase transition around 8 GPa is followed by an anomalous increase in the orthorhombic strain and tilt angle associated with the R point. Ab-initio calculation of the enthalpy in the various phases of $NaNbO_3$ is able to predict the phase transition pressure well [6].

Chemical and Particle Size Induced Phase Transition

The properties of materials can be tailored by chemical substitution. This technique has been found to be of special technological significance for preparing new devices. To investigate chemical substitution induced structural phase transitions, we have selected the solid solution $Li_xNa_{1-x}NbO_3$ with x=0.06 and 0.12 [8-10].

We have also investigated the structural phase transitions in $Li_{0.12}Na_{0.88}NbO_3$ (LNN12) in detail using the high temperature neutron diffraction techniques and determined in detail the phase diagram of this important material. We observed interesting changes with the appearance or disappearance of the super-lattice reflections in the powder diffraction patterns [figure 3 (a)]. This clearly reveals that LNN12 undergoes hitherto unreported structural phase transitions as a function of temperature. We infer that anomalies in dielectric measurements as reported in the literature correspond to successive phase transitions from orthorhombic O2 (***Pmc2$_1$***) to O1 (***Cmcm***) to tetragonal (***P 4/bmb***) to cubic (***Pm3m***), respectively. Subsequently, we suggest that the application of chemical pressure as a result of Li substitution in $NaNbO_3$ matrix favors the freezing of zone centre phonons over the zone boundary phonons that are observed in pure $NaNbO_3$.

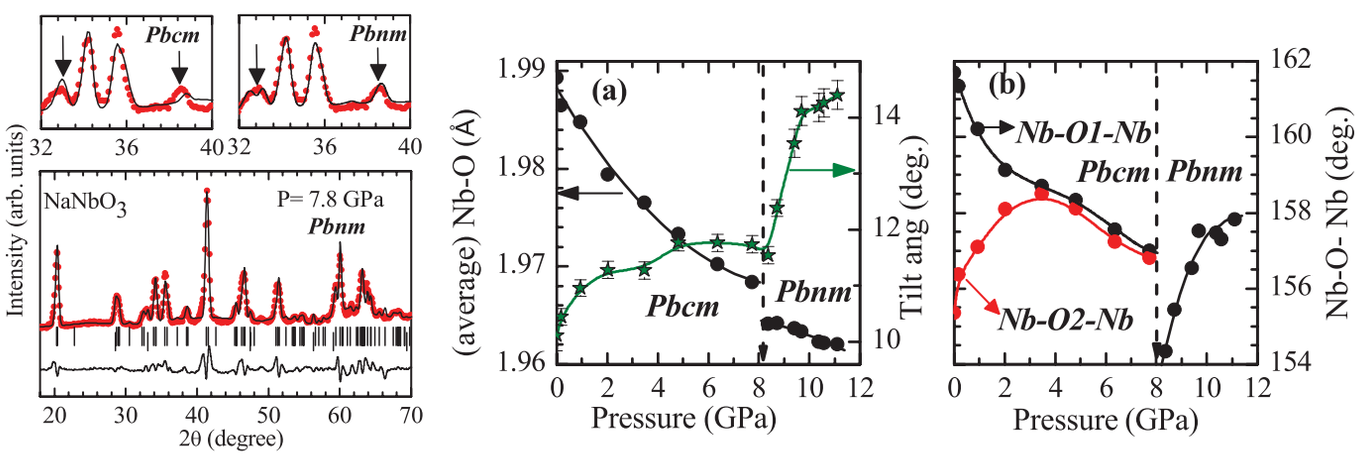

Fig. 2: (Left panel) Observed (circle), calculated (continuous line), and difference (bottom line) profiles [6] obtained after the Rietveld refinement of $NaNbO_3$ using orthorhombic *Pbnm* space groups at 8.7 GPa and 300 K. The arrow shows the accountability of superlattice reflection. Inset shows non-accountabilities of the characteristic reflections using orthorhombic *Pbcm* space group. (left and middle panel) Variation of the (a) Nb-O bond length (average), tilt angle associated with R point (q= ½ ½ ½) and (b) Nb-O-Nb bond angles for $NaNbO_3$ with pressure.

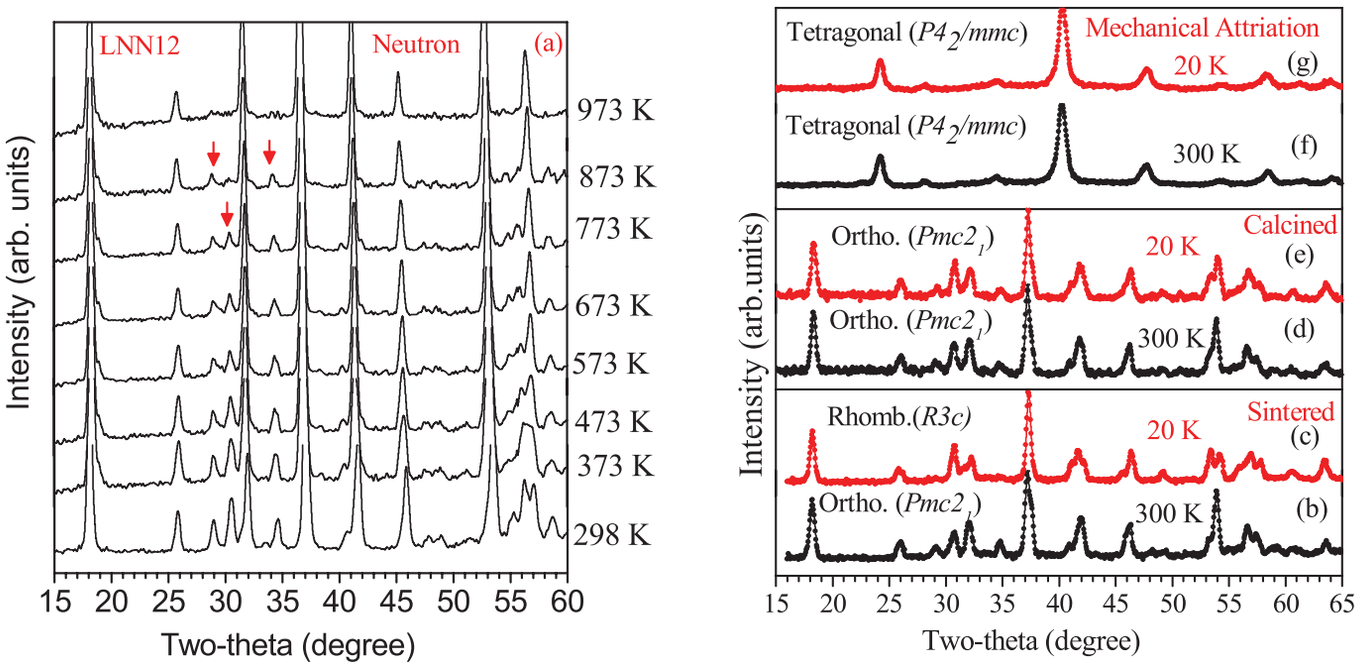

Fig. 3: (a) Evolution of powder neutron diffraction patterns [8] for $Li_{0.12}Na_{0.88}NbO_3$ (LNN12) with temperature. As temperature is lowered from 1073 K, it undergoes a phase transition with the appearance of additional superlattice peaks (marked with arrows). Right side panel shows the comparison of powder neutron diffraction data [9] for $Li_{0.06}Na_{0.94}NbO_3$, ((b) and (c)) sintered, ((d) and (e)) calcined, and ((f) and (g)) after mechanical attrition for 220 h at 300 K and 20 K, respectively.

We provide direct experimental evidence of a ferroelectric to paraelectric phase transition in ($Li_{0.06}$ $Na_{0.94}$) NbO_3 with reduction of particle size using a combination of x-ray and neutron powder diffraction techniques at room temperature. Detailed Rietveld analyses of the x-ray data shows variation of the particle size from micrometer to nanometer for sintered, calcined, and ball milled powders. The ferroelectric orthorhombic phase of micron sized powder (1.2 μm) is found to transform to paraelectric phase by reducing the particle size to 11 nm. The crystal structure of the paraelectric phase has been identified with tetragonal symmetry (***$P4_2/mmc$***) and is found to be a post perovskite phase. The low temperature neutron diffraction studies on the powders with different particle sizes reveal that the orthorhombic to rhombohedral phase transition gets suppressed with reducing particle size (Figure 3 right panel).

Phonon Dynamics and Phase Transition

Virtually all perovskites exhibit the high-symmetry cubic structure at high temperatures. The superlattice reflections observed in diffraction patterns originate from the condensation of zone-centre and zone-boundary soft phonon modes. Thus, the stability of various crystallographic phases could be understood in terms of phonon instabilities.

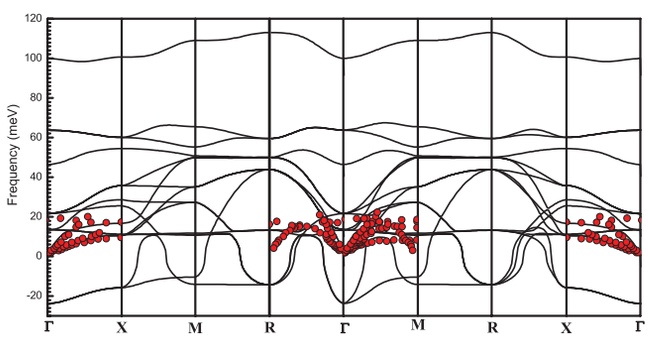

Fig. 4: Computed phonon dispersion relations [7] for cubic phase (*Pm3m*) of $NaNbO_3$ compared to reported experimental inelastic neutron scattering (INS) single crystal data (red circles) (see Ref. 7).

In order to detect these phonon instabilities using first principle technique, we have calculated the phonon dispersions from the zone centre () to the zone boundary points R and M (Figure 4). We found that the polar instability strength at the point is stronger than the antiferrodistortive instabilities at the R and M points, and the instability extends over a wider region of the Brillouin zone. As explain above, the R and M point soft phonons involve the anti-phase and in-phase tilting of adjacent oxygen octahedra respectively. Further, the strength of the M and the R point instabilities are quite similar. Interestingly, the branches along the -R and -M directions, show dramatic changes when reaching the R and M points. When moving away from M to R, two unstable modes are detected. One of them is rather flat and the other one shows rapid stiffening and becomes stable. Moreover, one of the stable modes becomes unstable at T (½, ½ ,¼) point.

Above 950 K, $NaNbO_3$ occurs in the cubic phase. On decreasing the temperature, it transforms to a tetragonal phase (***P4/mbm***). The structural transformation is from the cubic to tetragonal structure, where the unit cell is doubled in the plane perpendicular to the rotation axes of the M_3 mode. By further lowering the temperature, condensation of the R –point phonon leads to the orthorhombic ***Cmcm*** (T_2) phase. Unstable phonon-branches along the M-R line contribute to the occurrence successive phase transitions. These phonons play an important role in stabilizing the different phases (P, S and R) in $NaNbO_3$. We have proposed [7] that the additional

superlattice reflections are due to the condensation of the zone boundary phonons at T (**q**= ½, ½, g). The orthorhombic structures of the S, R and P phases result from the condensation of the phonon modes (q= ½, ½, g); with g= 1/12, 1/6 and 1/4. These orthorhombic phases originate from the modulation of the high symmetry cubic phase, associated with the phonon modes at **q**= (½, ½, g). Further, the freezing of the R- point phonon mode and a zone-centre phonon stabilizes the low-temperature ferroelectric rhombohedral phase. Based on our calculation we are able to assign the characteristic Raman modes in the antiferroelectric phase, which are due to the folding of the T (=95 cm^{-1}) and (=129 cm^{-1}) points of the cubic Brillouin zone, to the A_{1g} symmetry.

Conclusion

Powder Neutron scattering technique has been used to study variety of phase transitions under various thermodynamical conditions like temperature, chemical substitution and pressure in $NaNbO_3$. These transitions are characterized by the appearance and disappearance of superlattice reflections in the powder diffraction patterns. The superlattice reflections originate from the condensation of zone-centre and zone-boundary phonon modes. The stability of various crystallographic phases could be understood in terms of phonon instabilities.

References

1. M. E. Lines and A. M. Glass "Principles and Application of Ferroelectrics and Related Materials" (oxford: Clarendon, 1977); Xu. Yuhuan, Ferroelectric Materials and Their Applications (Nort-Holland Elsevier Science, 1991); L. G. Tejuca and J. L. G. Fierro "Properties and Applications of Perovskite-Type Oxides" (New York: Dekker, 1993).
2. E. Bousquet, M. Dawber, N. Stucki, C. Lichtensteiger, P. Hermet, S. Gariglio, J. M. Triscone and P. Ghosez, Improper ferroelectricity in perovskite oxide artificial superlattices Nature 452, 723 (2008).
3. Y. Saito, H. Takao, T. Tani, T. Nonoyama, K. Takatori, T. Homma, T. Nagaya, M. Nakamura, Lead-free piezoceramics, Nature 432, 84 (2004); E. Cross, Materials science: Lead-free at last Nature 432, 24 (2004).
4. S. K. Mishra, N. Choudhury, S. L. Chaplot, P. S. R. Krishna and R. Mittal, Competing antiferroelectric and ferroelectric interactions in $NaNbO_3$: Neutron diffraction and theoretical studies, Phys. Rev B 76, (2007) 024110 and reference therein.
5. S. K. Mishra, R. Mittal, V. Y. Pomjakushin and S. L. Chaplot, Phase Stability and structural temperature dependence in sodium Niobates, Phys. Rev B 83, (2011)134105.
6. S. K. Mishra, M. K. Gupta, R. Mittal, S. L. Chaplot and T Hansen, Suppression of Antiferroelectric state in $NaNbO_3$ at High Pressure from In Situ Neutron Diffraction, Appl. Phys. Lett. 101 (2012) 242907.
7. S. K. Mishra, M. K. Gupta, R. Mittal, M. Zbiri, S. Rols, H. Schober and S. L. Chaplot, Phonon dynamics and inelastic neutron scattering of sodium niobate, Phys. Rev. B 89 (2014) 184303.
8. S. K. Mishra, P. S. R. Krishna, A. B. Shinde, V. B. Jayakrishnan, R. Mittal, P. U. Sastry and S. L. Chaplot, High temperature phase stability in $Li_{0.12}Na_{0.88}NbO_3$: A combined powder X-ray and neutron diffraction study J. of Appl. Phys. 118, (2015) 094101.
9. S. K. Mishra, A. B. Shinde and P. S. R. Krishna Effect of particle size and strain on phase stability of $(Li_{0.06}\ Na_{0.94})\ NbO_3$, J. of Appl. Phys. 115, (2014) 174104.
10. S. K. Mishra, A. B. Shinde and P. S. R. Krishna, Response to comment on "Effect of particle size and strain on phase stability of $(Li_{0.06}\ Na_{0.94})\ NbO_3$, J. of Appl. Phys. 116, (2014) 206102.

Machine Vision Applications for Physical Security, Quality Assurance and Personnel Dosimetry

S. Kar, S.V. Shrikhande and R.M. Suresh babu
Electronics & Instrumentation Systems Division

Machine vision is the technology used to provide imaging-based solutions to variety of applications, relevant to nuclear facilities and other industries. It uses computerized image analysis for automatic inspection, process control, object sorting, parts assembly, human identity authentication, and so on. In this article we discuss the in-house developed machine vision systems at EISD, BARC for three specific areas: Biometric recognition for physical security, Visual inspection for QA of fuel pellets, and Fast neutron personnel dosimetry. The advantages in using these systems include objective decision making, reduced man-rem, operational consistency, and capability of statistical quantitative analysis.

Introduction

As the subject name suggests, Machine Vision (MV) deals with imparting the capability of vision to a machine in order to empower it so as to mimic human visual capability. MV is the technology to provide imaging-based solutions. It makes use of computerized analysis of images for automatic inspection, counting of particles, robotic guidance, precision alignment, pick & place, parts assembly, social welfare, human identity authentication and so on. The scope of MV is broad and emerging further with unfolding of novel usage. In this article we discuss the in-house systems developments at EISD, BARC for deployment of MV in three specific areas: Biometric assisted subject recognition for physical security, Visual inspection for quality assurance of nuclear fuel pellets, and Fast neutron personnel dosimetry.

MV System for Security

Biometric Identification

As the concern for security is increasing in society, the significance of making use of biometrics to establish personal identity and to detect impostors is increasing. Biometrics is the automated use of *physiological characteristics* or *behavioral traits* to determine or verify the identity of a person. As the chosen mode of biometric, Face Recognition (FR) technique has the advantages of easy client acceptance, straight forward imaging processing, being most natural in our day to day life and low marketing cost.

FR has drawn considerable attention globally amongst the research community in recent past. For the sake of testing the worth of various algorithms/systems provided by different companies/academia, a FR Vendor Test[3] (FRVT) was conducted by NIST, USA in 2013. Applications of FR include identity authentication for Homeland security as adopted by many national governments. Face forms part of Unique IDentification (UID) database built in India.

In order to achieve higher degree of security in the process of establishing identity, researchers around the globe have suggested various methods including use of multi factor authentication, multiple sensor based capture of signature (like utilizing visual & thermal zone of the spectrum), and multi biometric fusion (e.g. face, finger print & voice). In EISD, we have developed a face based uni-modal biometric system, and we are in the process of making a multi-modal system combing three different signatures extracted from hand. Both these systems are described blow.

Face Recognition System (FRS)

Development of Face Recognition System (FRS) was taken up[6] for carrying out automated recognition of subjects. FR process carries out facial detection, alignment & feature extraction, before matching an unknown face in a reference database of previous enrolments. An Imaging set-up (Fig.1a) with lighting arrangement was developed that restricts the inadvertent and inevitable variations occurring due to ambient effects during acquisition of the facial image, while maintaining a good image quality. Various facial matching techniques, e.g., Correlation, Principal Component Analysis (PCA), Discrete Cosine Transform (DCT), Hidden Markov Modeling (HMM) and Multi Algorithmic Fusion were tried out for performance evaluation before concluding suitability of the HMM approach due to its inherent robustness against the unavoidable data variations. The FRS has been configured for visitor entry processing (Fig.1b). This system comprises of a Visitor Entry Station, Imaging Booth, Pass Issue Station (carrying out visitor screening based on FR outcome), Supervisor Station, and Visit Conclusion Terminal. Application software modules were developed for each of the stations based on client server architecture. The system verifies whether the concerned subject ever visited earlier, thus detecting any possible attempt of entry in multiple identities. The system showed facial matching speed of $\approx$ *2.4 sec* with a reference database of 8,000 using a standard PC (with Intel(R) Core (TM)2 Duo CPU E7500@2.93GHz Processor) as host. The FRS is presently installed at CISF post near BARC North Gate for field trials.

Fig.1: (a) FRS Imaging Set-up.

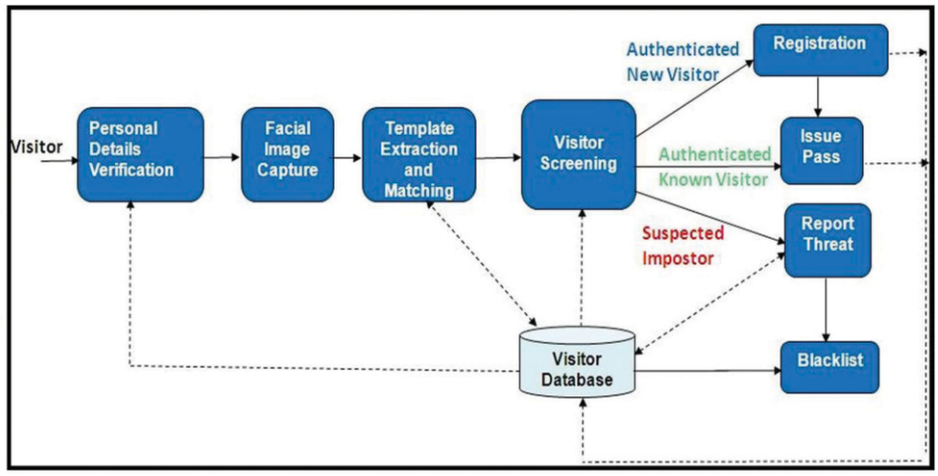

Fig.1: (b) FRS Configured for Visitor Management.

Hand based Multi-biometric Fusion

False-negative events (mistaken/wrong rejections) are always irritants to the users, and it impedes deployment of bio-metric for security. The false negative rates can be considerably reduced by multi-biometric fusion, which tolerates occasional single erroneous mismatch. Earlier we had developed a system that employs simultaneous matching of the multiple and distinctive 2-D image patterns on fingers from nail side of the hand at predefined positions, named as Hand Scan Biometric System (HSBS); the same was granted Indian Patent[2] No. 255627 dated 11/03/2013.

Under XII Plan, we have developed a Multi-biometric fusion based system (Fig.2b) for personnel identification with higher level of confidence, using Hand scan[1], Hand geometry, and Palm print as basic modalities. Fig.2a depicts the scheme for fusion. Presently the hand based fusion system is undergoing hardware testing and software integration in the lab. After performance validation, the system will be deployed at MFD, BARC for field trials.

Performance

Facial images used for evaluation are constrained to be in frontal pose with neutral expression, free of undesired variations as per ISO 19794-5 specifications. In order to finalize a facial matcher, we compared performance of three algorithms - PCA, DCT & HMM – employing about 1500 faces taken from the BioID database. Fig. 3 shows the results in terms of bar-graph depicting the recognition rate of the three algorithms for up to top 4 facial matches. HMM has the highest recognition rate for all the ranks.

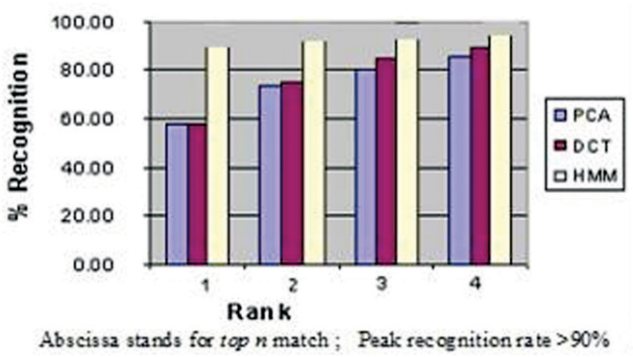

Fig.3: Comparison of PCA, DCT & HMM.

Three performance indices are used to assess a FR system: True positive (TP) rate (% correctly recognised); False positive (FP) rate (% wrongly recognised), and False negative (FN) rate (% wrongly rejected). Since the recognition decision

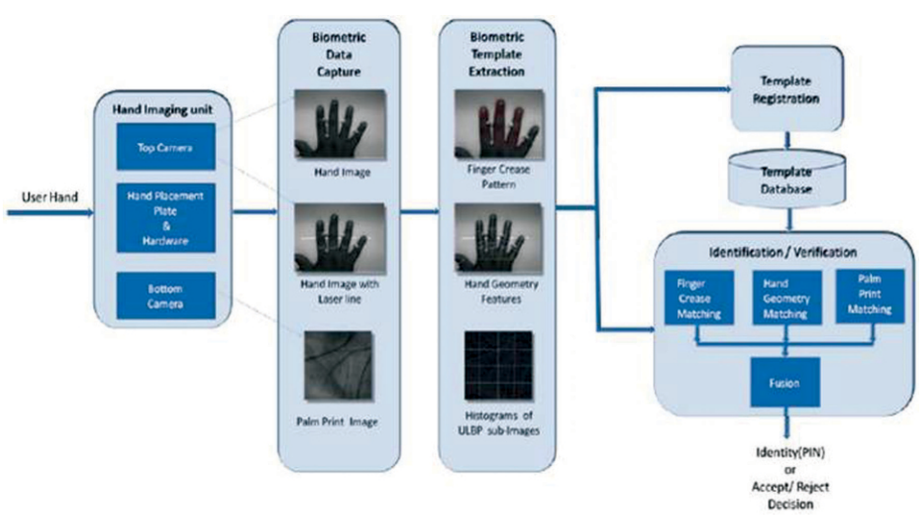

Fig. 2: (a) Scheme for hand based Multi-biometric Fusion.

Fig. 2: (b) Biometric Fusion unit.

is done based on a score, the algorithm uses a Threshold on score beyond which a positive result is decided. We have chosen a threshold that balances TP rate with FN rate. Field Trials of the FRS at CISF Site near BARC North Gate carried out between November, 2016 and January, 2017 revealed a TP rate of 99.08% with no false positive, computed over about 2000 test images, with 314 personnel registered with the system.

The HSBS was installed at three labs in BARC for trials and evaluation. Performance evaluated on 10,000 samples of 130 individuals revealed FN rate of <2% without any case of FP. After thorough lab testing, we observed near zero FP rates of HSBS. This development was deemed suitable for applications in the areas of access control to high security zones.

MV System for Quality Assurance (QA)

Automatic Pellet Inspection System (APIS)

APIS is developed for RMD, BARC for inspection of FBTR fuel pellets. The integrity of fuel pellets is very critical for proper stacking of pellets in fuel pin & expected heat transfer profile. Currently, surface inspection of pellets is done manually. This causes radiation exposure to humans and inconsistent inspection due to human fatigue. Automation aids in increased accuracy, consistency, productivity and deployment in harsh environments.

Fig. 4: (a) Pellet imaging set up.

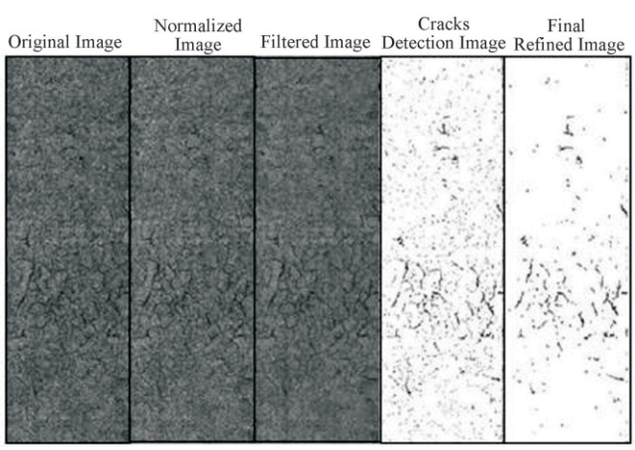

Fig. 4: (b) Various stages of image pre-processing.

FBTR Pellet is cylindrical in shape having 4.2 mm diameter and 7 mm length. The system (Fig.4a) uses a line scan camera and two area scan cameras to capture all three surfaces of the pellet. It uses an in-house developed pattern recognition and defect identification software to detect various types of defects such as Edge Chips, Multiple Body Chips, Singular Body Chips, Pits, Inclusions, Body Cracks, Left End Cracks, Right End Cracks, Longitudinal Cracks, Branch Cracks and Body Crazing. Fig. 4b shows typical pre-processing carried out for crack identification. Defect with dimension as small as 100 micron can also be identified. APIS consists of Imaging system, Pellet Handling machine, Control Electronics & Industrial PC.

The developed GUI provides online display of inspection status, maintains history, and supports post inspection analysis and offline analysis of acquired images. GUI also supports testing & troubleshooting of the machine and vision systems. It allows for configuration for settings of cameras, stepper motors and defect specifications. The system provides statistics of various types of defects, which helps in identifying the corrective measures for increased productivity.

The complete cycle of defect identification and segregation takes about 20 sec per pellet. The system has been tested, validated by the user and is ready for installation at RMD.

MV for Fast Neutron Dosimetry

CR-39 based Solid State Nuclear Track detectors (SSNTD) are used in India[5] for fast neutron personnel dosimetry. Based on the requirement for automating the process of counting the tracks generated in CR-39 detectors by exposure to fast neutron, the count being a measure of radiation dose received by the personnel wearing the detector foil, a MV system[4] was developed by EISD. Automating the counting process eases the burden of tedious manual work load, apart from making it precise, fast and accurate. The developed system (Fig.5d) is commissioned in the labs of RP&AD, BARC. In fact, this is the only lab in India where fast neutron dose measurement is done, with samples from around 2800 radiation workers (belonging to 70 DAE & Non-DAE institutions) received on quarterly basis.

The system is capable of processing a stack of 100 foils together, rendering the measurement process elegant and efficient. The automatic counting software of this system is empowered with the capability to resolve partially overlapping tracks, which are commonly found in foils exposed to higher levels (above 3 mSv) of neutron dose.

Fig.5a shows a typical CR39 foil (after exposure to fast neutron radiation) as imaged by the Dosimetry System. Fig. 5b illustrates the segmentation results obtained from 5a. The isolated tracks appear in green, overlapping tracks in red, and tracks generated from scratches, etc. in blue. Only the green tracks account for measured dose. The plot in Fig. 5c suggests a linear relation between computed track density (tracks in unit area) and received dose.

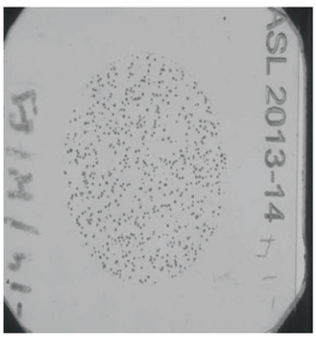

Fig. 5: (a) Original Image

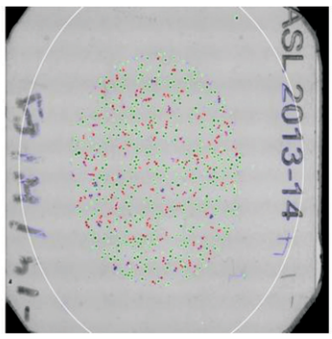

Fig. 5: (b) Processed Image

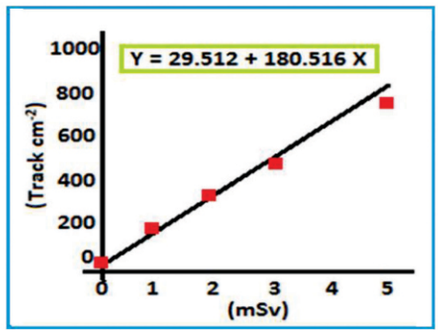

Fig. 5: (c) Track density vs. dose

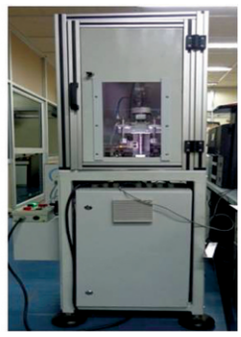

Fig. 5: (d) Neutron Dosimetry System

Challenges Faced

In case of FRS, dissimilarity in a single person's face from instance to instance can be very large, while that between different faces might be quite small. The ubiquitous data variations (Pose, Illumination, Expression ¬ together known as PIE) make the task of accurate FR very difficult in real life. In order to prevent spoofing of FRS, a way for 'live check' is required to be incorporated into the system. System scalability with increasing number of registrations is another major issue. In APIS, pellets being small and reflective, getting good quality image, especially considering the space constraint (for accommodating the cameras in the existing machine to be placed inside glove box), is an extremely challenging task. In case of Neutron Dosimetry, exposure of the foil to higher levels (particularly above 5 mSv) causes the tracks to overlap, rendering track counting inaccurate. Intelligent software with the capability to resolve the overlapping tracks is beneficial to reasonably compensate this factor.

Future Plan

In another application of MV, EISD is developing a system for conducting fracture test of piping components under Component Integrity Test Program pursued by RSD, BARC. Under this program, experiments will be conducted on Carbon Steel/Stainless Steel pipes. Using video images from camera, the crack length propagation is to be measured against the load values, employing Image Analysis (IA) techniques.

Conclusion

Visual sensing by machine is useful in many automation applications since it mimics the human sense of vision and allows for non-contact measurement of the environment. Adoption of Video Analytics proves helpful for performance improvement in FR systems. Multi-biometric Fusion improves accuracy, enhances performance, deters spoofing, and provides fault tolerance. In the present scenario of increased terrorist threats, it is highly prudent to deploy technology based solutions such as MV systems for identification, authentication and surveillance for reducing the human casualty and increasing the efficiency. In-house developed system has the advantage of total control on the hardware and software, unlike a commercial system, which is a black box with scant assurance that it does not contain any unwanted functions and that it will work correctly under all circumstances.

Acknowledgement

We sincerely thank Ms. Lizy P., Ms. Valli K., Ms. Swati H., Mr. K.Y.V. Krishna, Mr. P. Shah, Mr. A. Wadnerkar, Mr. P. Rajasekhar, Mr. R. Babu, Mr. S.S. Gaikwad of EISD, Dr. A.K. Bakshi, Ms. Rupali P. of RP&AD, Mr. S.D. Raut of RMD, R.K. Mittal of ED&DD for their participation and valuable feedback with suggestions for improvements during implementation of the MV systems.

References

1. Shah P. et al.; "Automated Hand Registration for Patented Finger Crease Pattern based Biometric Recognition"; *IEEE International Conference* WiSPNET 2017.
2. "A Biometric Method and System for Personal Identification using Multiple Patterns on Nail side of Fingers"; *Indian Patent No. 255627* dt. 11/03/2013.
3. FRVT'13 by NIST, USA: http://www.nist.gov/itl/iad/ig/frvt-2013.cfm
4. Pankaj S. et al.; "Automated Image Analyzer for batch processing of CR-39 foils"; *National Symposium on Nuclear Instrumentation* (NSNI-2013); BARC, Mumbai, 2013.
5. Rupali P. et al.; *Present status of Fast Neutron Personnel Dosimetry System based on CR-39 Solid State Nuclear Track Detectors*; *BARC Report BARC/2011/E/015, 2011.*
6. Rajesh B. et al.; "Performance Improvement of HMM based Face Recognition"; *National Conference on Machine Vision and Image Processing* (NCMVIP-2011), 2011.

Sixteenth Training Course on "Crane Operation", organised by Material Handling Equipment Committee of BARC Safety Council

Material Handling Equipment (MHE) Committee under Conventional & Fire Safety Review Committee (CFSRC) conducts regular training courses on "Crane Operation" and "Crane maintenance" to impart general awareness on industrial safety, safe practices to follow for crane operation, regulatory requirements, fault diagnosis and maintenance of EOT cranes for the staff of DAE. The 16th training course on Crane Operation in DAE and 2nd at Tarapur was conducted at Tarapur during 7 – 10 November, 2016 for the Technicians and Scientific Assistants of BARC, Tarapur and Trombay.

The training course was inaugurated on November 7, 2016 at TRP auditorium. Shri P. G. Behere, Chief Supdt., AFFF welcomed the dignitaries and the participants to the function. Shri S. Rajendran, Member-Secretary, MHE Committee briefed the role of MHE Committee at different stages of procurement process, periodical inspection, testing & certification of MHE in his introductory remarks. Shri Y. K. Taly, Chairman, BSC delivered the inaugural address. He explained SAHARA (Safety as High as Reasonably Achievable) principle and the importance of training to the operators to achieve accident free environment. Compiled lecture notes were released at the end. The inaugural function was also graced by Shri R. B. Bhatt, Plant Supdt., AFFF and Shri S. Ramasubramanian, Deputy Plant Supdt., TRP. The MHE Zonal Coordinator, Shri Dilip Kumar proposed vote of thanks.

The course was attended by 38 participants (25 from BARC, Tarapur and 13 from BARC, Trombay). It was carried out through classroom lectures in the forenoon and hands-on training to operate the crane in the afternoon. A site visit to Spent Fuel Storage Facility (SFSF) was also arranged to the participants. Faculties of the course were members of MHE Committee.

The training course covered introduction to MHE, mechanical & electrical components of EOT crane; roles and responsibilities of crane operators; pre-operational, operational and post-operational checks of EOT crane; personal protective equipment and safety in material handling & storage; single failure proof crane and in-cell crane under the subject "special material handling equipment" and regulatory requirements for MHE. A lecture on first-aid was delivered by Tarapur hospital staff to provide initial assistance to the victim during various emergency situations. A written test was conducted at the end of the course.

All the candidates passed the examination and the certificates were distributed during valedictory function held on November 10, 2016. Shri R. B. Bhatt, Plant Supdt., AFFF inaugurated the function. Shri S. Pradhan, Chief Supdt., TNRPO & Director, GSO delivered the valedictory address. He appreciated MHE Committee for its efforts to impart safety awareness to the crane operators. Shri P. G. Behere in his keynote address appreciated the course content and highlighted the hazards involved in handling nuclear materials. Guest of honour Shri K. Jayarajan, Head, BSCS informed that majority of accidents occur due to negligence and reiterated the importance to proper training. Feedback on the training programme was taken from the participants for improving the future training programmes. The training programme was well appreciated by all the participants.

(a) (b) (c)

Hands-on training given to the trainees to handle the material using EOT Crane at TRP Workshop, Tarapur (a) Rigging practice (b) Moving pipe in horizontal direction in close proximity (c) Upending of pipe

Technology Transfer to Industries

Between August and October 2016, Technology Transfer & Collaboration Division, BARC transferred eight technologies to various industries.

A. "Cr (VI) DK: Chromium (VI) Detection Kit For Water" Technology:

This technology was developed by the National Centre for Compositional Characterization of Materials (NCCCM), Hyderabad, Chemistry Group. Chromium, especially Cr (VI) is highly carcinogenic and needs regular monitoring in drinking water due to its extensive use in various industrial process and possible release to environment. As per Indian standard IS 10500 for drinking water, the maximum permissible contamination of Cr (VI) in drinking water is 50µg/L. Using the Chromium (VI) detection kit water samples can be easily categorized as being safe, permissible or toxic for drinking from chromium (VI) point of view.

This technology was transferred to M/s LTEK Systems, Nagpur, Maharashtra.

B. "Solar Powered Portable Domestic Brackish Water Reverse Osmosis (BWRO)" technology:

"Solar Powered Portable Domestic Brackish Water Reverse Osmosis (BWRO)" technology was developed by Desalination Division, BARC. It has a capacity of 10 litres/hr (lph) which can bring down the salinity of water from 1000 - 3000 ppm (mg/lit) to 50 - 300 ppm and will be free from toxic elements, pathogens and turbidity.

This technology was transferred to M/s Dantal Hydraulics Pvt. Ltd., Gurgaon, Haryana.

C. "Arsenic Removal from Drinking Water by Ultrafiltration Membrane Assisted Process" Technology:

Arsenic (As) is very toxic element and a carcinogen The World Health Organization's guideline for arsenic in drinking water is 10 parts per billion (ppb). In India, states like Uttar Pradesh, Bihar, Jharkhand, West Bengal, Assam, Manipur, mainly in Ganga-Meghna-Brahmaputra belt with a population of over 500 million have reported serious illnesses due to presence of arsenic in groundwater. An Ultrafiltration (UF) membrane assisted physicochemical process for removal of arsenic from ground/surface water was developed by BARC to make the water safe for drinking.

This technology was transferred to M/s Awatech Solutions (I) Pvt. Ltd., Ahmedabad, Gujarat.

D. "On-Line Domestic Water Purifier Based on Ultrafiltration Polysulfone Membrane" Technology:

This technology was developed by Membrane Development Section, Chemical Engineering Group, BARC. The "on-line domestic water purification device" is based on polysulfone ultrafiltration membrane in a unique cylindrical configuration.

The technology was transferred to M/s Aquacare Industries, Pune, Maharashtra.

E. "Partially hydrolyzed guar gum for dietary fiber applications" Technology

Dietary fibers are an important nutritive component. Guar gum, which is derived from seeds of legume plant, is widely used as thickener in food products. Guar gum needs to be depolymerized to be used as dietary fiber. Present technology details process for purification and subsequent radiation processing of guar gum to obtain partially hydrolyzed guar gum for use as soluble dietary fiber. This process is an alternative to the presently used enzymatic process of depolymerization.

This technology was transferred to M/s Veena Industries, Nagpur.

F. "Seismic Switch (Analog and Digital)":

Seismic Switch (Analog) can accurately detect of strong earthquakes and provides a safe shut down option for various Industrial Processes.

It monitors acceleration in all the three axes and triggers on detection of Peak Ground Acceleration (PGA). Trimpots are provided for easy threshold settings. The unit provides Earthquake relay and Status relay. Earthquake relay is in energised state during normal operation and de-energises on complete loss of power to ensure 'fail safe' operation of the system. On-line testability is another important feature in this system which enables the user to manually initiate the self-diagnostics of the system without removing it from the installation. Battery backup provides for 10 hrs of power. IP66 enclosure makes the system robust for all environments.

Seismic Switch (Digital) is packed with many distinctive features specially designed for meeting the standards for nuclear industries. This is helpful in highly accurate detection of a strong earthquake or a structural vibration with various safe shut down options.

It monitors acceleration in all the three axes and triggers on detection of Peak Ground Acceleration (PGA) on any axis.

The unit provides two numbers of 2 Form C (DPDT) isolated relay contacts. Relay 1 (Earth quake relay) and Relay 2 (Status relay). Coils of both these relays are in energised state during normal operation and de-energises on any fault. This ensures 'fail safe' operation of the system. On-line testability is another important feature in this system which enables the user to manually initiate the self-diagnostics of the system without removing it from the installation. Seismic Switch (Digital) can communicate to a Graphical User Interface Software through an RS-485/RS-232 link. Various features of this software include remote reset for automatic leveling, self test, password protected access, saving instrument details in EEPROM, setting trip parameters, display of battery status, real-time plots of accelerations and display of various other system parameters such as voltage and temperature. The system can be programmed for having additional triggering conditions such as Cumulative Average Velocity (CAV).

The know-how of this technology was transferred to M/s ECIL, Hyderabad.

G. "Peripheral Pulse Analyzer"

The technology was developed by Electronics Division, BARC. It is a computer based system for the study of physiological variabilities. It has unique feature that it yields heart rate variability, respiration rate variability, cardiac output variability / peripheral blood flow variability from a single data acquisition session from the patient. The data acquisition is controlled by a PC, serially connected to the acquisition unit. The variability analysis and transfer to database is performed by the PC with the help of Peripheral Pulse Analyzer package in post processing module.

This technology was transferred to M/s Sanjeevani Electromedicals, Navi Mumbai.

H. MoU was signed for "Setting up of DAE Technologies Dissemination & Display Facility" in National Institute of Technology, Trichy and with Gitam University, Visakhapatnam, Andhra Pradesh.

I. With ACTREC, Kharghar, Navi Mumbai, an MoU was signed for "Development of New Cancer Therapeutics based on novel formulations of known therapeutic compounds".

J. MoU for "Setting up and operation of DAE Litchi technology demonstration cum treatment facility and centre of excellence (DLTF-CoE)" signed with Indian Council of Agricultural Research (ICAR), National Research Centre on Litchi (NRCL), Mushahari, Muzaffarpur, Bihar.

K. MoU for "Development of gold reference standard" signed with Indian government Mint (IGM), Mumbai and CSIR-National Physical Laboratory (NPL), New Delhi.

28th DAE All India Essay Contest

The 28th DAE All India Essay Contest on 'Nuclear Science and Technology' was held in October 2016. A total of 355 essays were received, out of which the authors of 36 essays were selected for making an oral presentations at DAE, Mumbai. The selected participants visited various DAE facilities such as BARC, TAPS-3&4, BRIT and Electron Beam Centre. Prizes in cash were awarded on Founder's Day celebrated on October 28, 2016 in BARC.

170 essays were received on "Nuclear Power in India – Challenges and Future Direction" out of which 12 were shortlisted. 81 essays were received on "Societal Benefits of non-power applications of nuclear science and technology" and 12 essays were shortlisted. 104 essays on "Laser Light in the service of Indian Nuclear Energy" were received and 12 were shortlisted from this category. The final winners in each listed below of the theme.

Topic – Nuclear Power in India – Challenges and Future Direction

Name	Student of	Place	Prize
Ankit Yadav	BE (Mech)	Roorkee	First
Ms. L S Aparna	BE (ECE)	Thrivananthapuram	Second
Sr. Deena David	BA (English)	Kottayam	Third

Topic – Societal benefits of non-power applications of nuclear science and technology

Name	Student of	Place	Prize
Ms. Pranshuta Bansal	MBBS	Jhalawar	First
Ms. Muhsina Jasmi P	B Sc (Chem)	Pulikkal (KL)	Second
Ms. Bhagyalaxmi Unnik'nan	B Sc	Ernakulam	Third

Topic – Laser Light in the service of Indian Nuclear Energy

Name	Student of	Place	Prize
G. Rajashekar	BTech (IT & Comp)	YSR Dist (AP)	First
Ms. Farha S	B Sc (Phy)	Palakkad (KL)	Second
Christo Robson	BE (Mech)	Chennai	Third

Release of the Founder's Day Special Issue of the BARC Newsletter

Founder's Day special issue of the BARC Newsletter was released by Director, BARC on 28th October, 2016 carrying 25 Award winning Papers, out of which 5 were from Homi Bhabha Science & Technology Awardees, 9 from Scientific & Technical Excellence Awardees, 5 from Young Applied Scientist / Technologist Awardees, 3 from Young Scientist Awardees, 2 from Young Engineer Awardees and 1 from INSA Young Scientist Awardee.

DAE (Excellence in Science, Engineering & Technology) Awards 2015

A. Homi Bhabha Science & Technology Awardees

1. Shri I.V.N.S. Kamaraju, SO/H, KBNRP&C, NRB, BARC

Shri Kamaraju has been awarded for his innovative research contributions in field of "*Erection and construction of different mechanical systems of Project PREFRE-3A, presently the largest reprocessing plant*". He has demonstrated his professional excellence in planning and executing the challenging task of high density piping work inside the confined process hot cell. One of his major achievements has been the completion of fabrication and erection of all 6200 pipe spools amounting to about 100 km of small bore (90% of pipes up to 25 mm NB) piping with 45000 RT qualified weld joints inside the confined hot cells with restricted access while maintaining high quality and safety standards.

2. Shri Rayakamath Dinesh Babu, SO/H, RPD, RPG, BARC

Shri Babu has been awarded for his contributions in the field of "*Core Calibration Experiments at P4 and development of reactor internals and equipment to be used in a project of national importance*". He has played a pivotal role in the core calibration campaign at P4, which was successfully completed due to his hard work, dedication, extensive field engineering and excellent coordination. He also has played a key role in developing infrastructure at site for refuelling and commissioning of novel Spent Fuel Storage Modules

3. Dr. P. K. Mukherjee, SO/G , NABTD, BSG, BARC

Dr. Mukherjee has been awarded for his contributions in the field of "*Agricultural research*". He has made significant contributions in understanding the biology of the most popular biofungicides Trichoderma spp. in improvement of strains using radiation-induced mutations, development of processes for formulations and in mining of Trichoderma genomes for novel metabolites and proteins of relevance to agriculture and medicine. He has transferred two technologies to five biotech companies.

5. Shri S. Sarkar, DS & Director, ChTG, BARC

Shri Sarkar has beem Awarded for his contributions in the field of "***Chemical Engineering*** ". He had led a multi-disciplinary team of Engineers and Scientists in harnessing multi-disciplinary *"Enrichment Technology*" to meet the growing strategic and non-strategic applications of the nation. He has immensely contributed and spearheaded the scaling up of in-house developed Fluorine production technology, plant scale refining of different kinds of feed materials, indigenous development of ultra-low range flow meters and vacuum gauges, development of advanced technology HSR machines with higher output and their successful deployment in larger scale.

6. Shri Kailash Agarwal, OS & GM, NRPSED & KNRPD, BARC

Shri Agarwal has been awarded for his contributions in the field of "*Development of Technologies for Reprocessing Facilities*". He also played a key role in development of new technologies for spent fuel storage and handling, hull monitoring, hull compaction and feed clarification, which resulted in enhanced plant performance. He had provided innovative and speedy solutions to many challenging problems during the first two years of PREFRE-2 operation. He has given shape to the concept of Direct Fuel Transfer from pool to spent fuel chopper, which eliminates the multiple handling of heavy charging casks.

7. Shri. Satish B. Patil, SO/F, TDD NRG, BARC & Smt. Jyoti Jha, SO/F, TDD NRG, BARC

Jointly awarded for outstanding contribution in the field of "*Design & Development of Facility for Production of Active Cs-137 Source Pencils for Blood Irradiator*". Shri. Satish Patil and Smt. Jyoti Jha have made excellent contribution in development of technology for utilization of Cs-137 recovered from nuclear waste as a radioactive source for medical applications. This achievement has placed Department of Atomic Energy, India at a new height in the international arena in terms of producing Cs-137 Source Pencils in the Vitrified form.

8. Dr. Ranjan Mittal, SO/H, SSPD, PG,BARC

Dr. Mittal has been awarded for his outstanding contributions in the field of "*Condensed Matter Physics, in particular, the experimental studies on neutron inelastic scattering and computational studies on lattice dynamics*". He has made significant contributions in Condensed Matter Physics in the area of neutron inelastic scattering experiments and computational lattice dynamics. He has carried out extensive phonon study on yttria, multiferroic and scheelite structured compounds to understand the role of structural distortions and their correlation to phonon instabilities, leading to phase transitions in these compounds.

B. Exceptional Service Awardee

Dr. R.K. Patil, Former Associate Director was instrumental in indigenous development of Control & Instrumentation systems. He was responsible in evolving the Control and Instrumentation for Dhruva Reactor from concept Stage and its implementation and integration. He has made significant contribution in C&I to various other DAE projects such as Purnima II & III Reactors, Kamini Reactors, PRP Reactor Program.

Central Complex at BARC

Edited & Published by:
Scientific Information Resource Division
Bhabha Atomic Research Centre, Trombay, Mumbai 400 085, India
BARC Newsletter is also available at URL:http://www.barc.gov.in